

Recent Advances in MOF-Based Adsorbents for Dye Removal from the Aquatic Environment

Mohammadreza Beydaghdari ¹, Fahimeh Hooriabad Saboor ^{1,*}, Aziz Babapoor ¹, Vikram V. Karve ² and Mehrdad Asgari ^{2,3,*}

¹ Department of Chemical Engineering, Faculty of Engineering, University of Mohaghegh Ardabili, Ardabil 56199-11367, Iran; m.beydaghdari@gmail.com (M.B.); babapoor@uma.ac.ir (A.B.)

² Institute of Chemical Sciences and Engineering, École Polytechnique Fédérale de Lausanne (EPFL), CH-1951 Sion, Switzerland; vikram.karve@epfl.ch

³ Department of Chemical Engineering & Biotechnology, University of Cambridge, Philippa Fawcett Drive, Cambridge CB3 0AS, UK

* Correspondence: f.saboor@uma.ac.ir (F.H.S.); ma2000@cam.ac.uk (M.A.)

Abstract: The adsorptive removal of dyes from industrial wastewater using commercially available adsorbents is not significantly efficient. Metal–organic frameworks (MOFs) offer outstanding properties which can boost the separation performance over current commercial adsorbents and hence, these materials represent a milestone in improving treatment methods for dye removal from water. Accordingly, in this paper, the recent studies in the modification of MOF structures in dye removal from the aquatic environment have been discussed. This study aims to elaborate on the synthetic strategies applied to improve the adsorption efficiency and to discuss the major adsorption mechanisms as well as the most influential parameters in the adsorptive removal of dyes using MOFs. More particularly, the advanced separation performance of MOF-based adsorbents will be comprehensively explained. The introduction of various functional groups and nanomaterials, such as amine functional groups, magnetic nanoparticles, and carbon-based materials such as graphene oxide and CNT, onto the MOFs can alter the removal efficiency of MOF-based adsorbents through enhancing the water stability, dispersion in water, interactions between the MOF structure and the contaminant, and the adsorption capacity. Finally, we summarize the challenges experienced by MOF-based materials for dye removal from water and propose future research outlooks to be considered.

Keywords: adsorptive separation; dye removal; functionalized MOF; MOF composite; water treatment

Citation: Beydaghdari, M.; Hooriabad Saboor, F.; Babapoor, A.; Karve, V.V.; Asgari, M. Recent Advances in MOF-Based Adsorbents for Dye Removal from the Aquatic Environment. *Energies* **2022**, *15*, 2023. <https://doi.org/10.3390/en15062023>

Academic Editor: Giorgio Vilardi

Received: 10 February 2022

Accepted: 3 March 2022

Published: 10 March 2022

Publisher's Note: MDPI stays neutral with regard to jurisdictional claims in published maps and institutional affiliations.



Copyright: © 2022 by the authors. Licensee MDPI, Basel, Switzerland. This article is an open access article distributed under the terms and conditions of the Creative Commons Attribution (CC BY) license (<https://creativecommons.org/licenses/by/4.0/>).

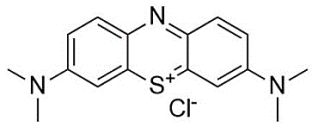
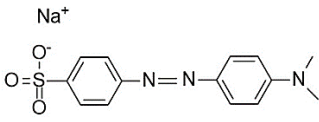
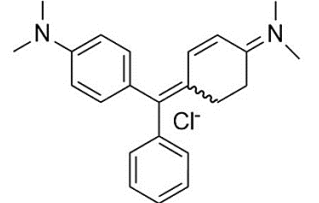
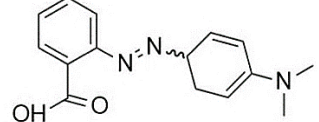
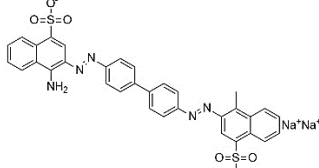
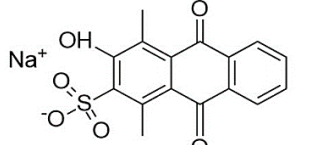
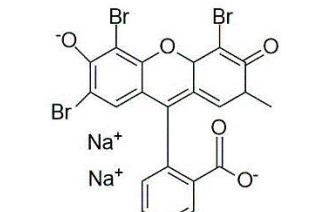
1. Introduction

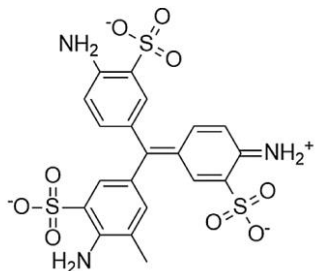
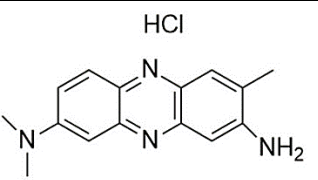
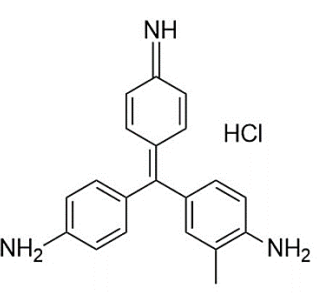
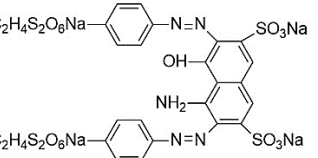
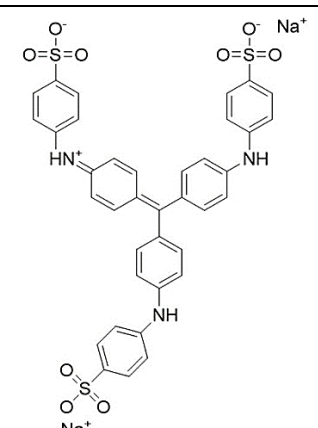
1.1. Dye Contaminants in the Aquatic Environment

Water is the most vital substance for life on earth; the health of all living things, including humans, plants, and animals depends on its existence. Water pollution and water scarcity are severe environmental problems worldwide, where one of the most critical challenges of human society is the conservation and proper use of water resources [1,2]. Industrial activities, daily activities of humans, agriculture, etc., cause water pollution. Hazardous substances in industrial wastewater endanger human life and aquatic organisms [3,4]. Access to safe and clean water is essential for various activities, and discharging effluents into the environment leads to a severe challenge to safe water accessibility. Various pollutants enter the environment and pollute water resources. One of the most toxic pollutants of water resources is dyes. Leather [5], textiles [6], paper and rubber [7], plastic [8], and food [9] are among the industries in which dyes have a wide range of applications. Over 1,600,000 tons of dyes are produced worldwide [10–12]. Dyes are usually classified

based on the structural or functional groups plus the ionic charge during dissolution in aqueous solutions [13]. Organic dyes in wastewater are toxic, carcinogenic, and may cause health problems such as respiratory problems, cyanosis, skin irritation, and headache [14]. In addition, the presence of dyes in water reduces dissolved oxygen in water and lowers sunlight irradiation to plants and organisms in water. Moreover, they cause bad odors due to the high chemical oxidation demand [15,16]. Accordingly, treatment of dye contaminant wastewater before discharging into the environment is necessary [17]. Some of the dyes mentioned in this research are presented in Table 1.

Table 1. Specifications of various dyes.

Dye	IUPAC Name	Molecular Formula	Molecular Mass (g/mol)	Chemical Structure
Methylene blue	[7-(dimethylamino) phenothiazin-3-ylidene]-dimethylazanium;chloride	C ₁₆ H ₁₈ N ₃ SCl	319.85	
Methyl orange	sodium;4-[[4-(dimethylamino) phenyl] diazenyl]benzenesulfonate	C ₁₄ H ₁₄ N ₃ NaO ₃ S	327.33	
Malachite green	[4-[[4-(dimethylamino)phenyl]-phenylmethylidene]cyclohexa-2,5-dien-1-ylidene]-dimethylazanium;chloride	C ₂₃ H ₂₅ ClN ₂	364.91	
Methyl red	2-[[4-(dimethylamino)phenyl]diazenyl]benzoic acid	C ₁₅ H ₁₅ N ₃ O ₂	269.3	
Congo red	1-naphthalenesulfonic acid-3,3'-(4,4'-biphenylene bis (azo)) bis (4-amino-) disodium	C ₃₂ H ₂₂ N ₆ Na ₂ O ₆ S ₂	696.67	
Alizarin red S	3,4-Dihydroxy-9,10-dioxo-9,10-dihydroanthracene-2-sulfonic acid	C ₁₄ H ₇ NaO ₇ S	342.26	
Eosin	2-(2,4,5,7-tetrabromo-6-oxido-3-oxo-3H-xanthen-9-yl)benzoate	C ₂₀ H ₆ Br ₄ Na ₂ O ₅	691.86	

Fuchsin acid	Disodium 2-amino-5-[(Z)-(4-amino-3-sulfonatophenyl)(4-iminio-3-sulfonato-2,5-cyclohexadien-1-ylidene)methyl]-3-methylbenzenesulfonate	$C_{20}H_{17}N_3Na_2O_9S_3$	585.54	
Neutral red	3-Amino-7-dimethylamino-2-methylphenazine hydrochloride	$C_{15}H_{17}ClN_4$	288.77	
Fuchsin basic	4-[(4-Aminophenyl)(4-imino-2,5-cyclohexadien-1-ylidene)methyl]-2-methylaniline hydrochloride (1:1)	$C_{20}H_{20}ClN_3$	337.85	
Sunset yellow	disodium 2-hydroxy-1-(4-sulfonatophenylazo)naphthalene-6-sulfonate	$C_{16}H_{10}N_2Na_2O_7S_2$	452.4	
Reactive Black 5	tetrasodium;4-amino-5-hydroxy-3,6-bis[[4-(2-sulfonatooxyethylsulfonyl)phenyl]diazenyl]naphthalene-2,7-disulfonate	$C_{26}H_{21}N_5Na_4O_{19}S_6$	991.8	
Methyl blue	disodium;4-[4-[[4-(4-sulfoanilino)phenyl]-[4-(4-sulfonatophenyl)iminocyclohexa-2,5-dien-1-ylidene]methyl]anilino]benzenesulfonate	$C_{37}H_{27}N_3Na_2O_9S_3$	799.81	

Various methods such as coagulation [18], membrane separation [19], adsorption [20], oxidation processes [21], solvent extraction [22], electrolysis [23], and biological processes [24] are used to purify wastewater and to reduce the dye concentration from the effluent before discharging into the environment. Among these methods, adsorption technology has been proposed as a popular, efficient, low-cost, fast, and easy method for treating dye wastewater [25,26]. A wide range of adsorbents are used for adsorption processes.

In this regard, finding new adsorbents or modifications of existing adsorbents for achieving higher adsorption capacity and better adsorption conditions has always been of interest [27,28]. Novel adsorbents under consideration should have high adsorption capacity, good stability in the aquatic environment, reusability, and low cost [29,30]. In this regard, MOFs have been introduced as high-performance adsorbents for dye removal applications [31].

1.2. Metal–Organic Frameworks

MOFs have been proposed as an essential part of porous nanomaterials in various applications such as adsorption and photocatalytic degradation [32], sensors [33], gas storage [34], energy conversion plus storage [35], and drug delivery [36] in recent years. MOFs can be synthesized with different dimensionality as well as different sizes and shapes, depending on the type of synthesis and raw materials used [37]. Due to its excellent performances in various applications in different fields, it has been considered an essential member of new porous materials in recent years. MOFs present excellent performance in removing various contaminants from the gaseous and aqueous medium [38]. The most important advantages of MOF over other adsorbents are structural diversity [39], the possibility of determining the size of the pores, as well as determining the properties and performance by selecting various metal nodes and organic ligands in the synthesis stage. Various methods such as solvothermal [40], hydrothermal [41], mechanochemical [42], sonochemical [43], spray drying [44], sol-gel [45], and flow chemistry [46] have been used in MOFs synthesis. Another advantage of MOFs over other adsorbents is the low energy required for the regeneration process [47], large surface area [48], as well as high thermal and mechanical stability [49].

In recent years, the adsorptive removal of various pollutants from the aquatic environment is a widely studied field of application of MOFs [50]. Among these, dyes are one class of pollutants tested in particular, as other conventional methods and adsorbents are ineffective in the removal of these pollutants from the aquatic environment. This article presents a comprehensive review on the properties of bare MOFs and optimized MOFs in the adsorptive removal of dyes. The following sections discuss MOFs' characteristics and performance as adsorbents, and recent advances on removing dyes from aquatic environments using MIL-type, zirconium-based MOFs, Zeolitic Imidazolate Frameworks (ZIFs), magnetic MOFs, amine-functionalized MOFs, and GO-MOF and CNT-MOF nanocomposites. Moreover, the effectiveness of pH, adsorbent dosage, contact time, initial dye concentration as the most important parameters on dye removal using MOFs are discussed.

2. Characteristics of MOFs as Adsorbents

2.1. The Structure of MOFs as Adsorbents in the Aquatic Environment

Metal–organic frameworks with a high surface area, ranging from 100 to 10,000 m²/g [51], are composed of metal ions and organic linkers [52–54]. Various MOFs with different structural properties can be created using different metal ions and organic ligands [55]. Organic ligands play an essential role in MOFs structures and in determining structural properties such as thermal stability, stability in the aqueous environment, and adsorption performance. The most widely used organic linkers are displayed in Figure 1. Organic ligands play an essential role in the higher adsorption capacity by creating symmetric pores. The lack of strong bonds between metal and ligand leads to poor stability of MOF in water. Stronger bonds between the linkers and the metal ions results in a more stable MOF in water. The hydrophobic nature of ingredients is important in the water stability of MOFs. The introduction of some functional groups such as alkyl and fluoride groups to the ligand also leads to a more stable structure in the aquatic environment [56,57]. Metal ions are also important in the stability of the MOF structure. The use of more than one metal ion in the structure can lead to MOF stability. This is because of the formation of more strong bonds compared to monometallic metal clusters. Reduction in the mobility

of the metallic cluster, reduction in the mobility of inorganic secondary building units, and introduction of intermolecular interactions such as π - π and hydrogen bonding have significant effects on the hydrothermal stability of MOFs [58].

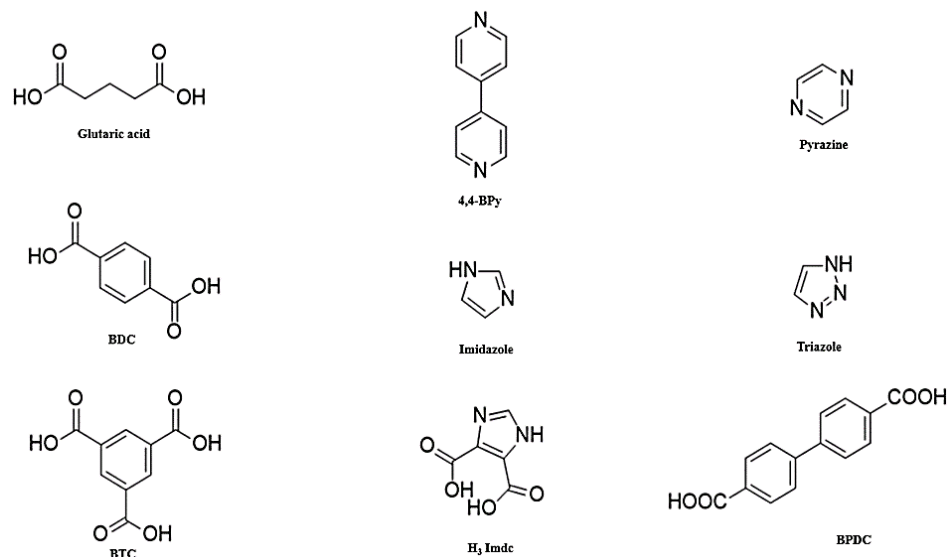


Figure 1. Structure of most common organic linkers used in the synthesis of MOFs; reprinted with permission from Ref. [59]. Copyright 2019 Elsevier.

MOFs can be applied to pollutant purification, including organic dyes, as one of the primary sources of water contamination. Some characteristics of MOFs make them appropriate materials for dye adsorption from wastewater with preferable performance over other conventional adsorbents [59]. These characteristics include crystalline, porous structure, large surface area, multifunctional capabilities, structural diversity, flexible structure, and very active sites for dye adsorption [60,61]. The porosity of the MOF structure improves the adsorption of pollutants into adsorption sites and facilitates the saturation of adsorption [62]. MOFs are superior materials for water treatment as their structural ligands provide a high density of adsorption sites and their ultrahigh porosity improves the extraction of pollutants from contaminant sources [63].

2.2. Adsorption Performance of MOFs in the Aquatic Environment

The adsorption and removal performance of pollutants by MOFs is almost similar to other adsorbents. However,

- (i) Open and active metal sites in MOFs can act as an additional adsorption site [63].
- (ii) Functionalized pores, which are able to perform specific host-guest interactions including electrostatic interactions [64], H-bonding [65], hydrophobicity [66], acid-base interactions [67], and π - π interactions. These interactions between MOF and contaminant molecules can improve the adsorption capacity [68].
- (iii) One of the necessary factors for high adsorption capacity and efficient adsorbent performance is the large surface area of the adsorbent. A large surface area has greater capacity to host polluting molecules and provides more active sites for contaminant uptake.

2.3. The Adsorption Mechanism of Dyes on MOF-Based Adsorbents

The mechanisms of dye adsorption by MOFs are similar to other adsorbents, except that the presence of ligand functional groups and the presence of metal ions or metal clusters in the structure of MOFs in some cases cause two or several interactions between dye and MOF, and performance improvements in the adsorption processes.

The most common interaction is the electrostatic interaction that occurs between two species with different surface charges. The electrostatic interaction is observable between a wide range of dyes and MOFs [65–67]. The π - π interaction is usually observed in the removal of compounds containing aromatic rings. Dyes such as MG, MO, and CR, which contain multiple aromatic rings, can interact with MOFs that have aromatic rings in their structure [64,68]. Hydrogen bonding is also observed between dyes and MOFs that can bond between hydrogen atoms and electronegative atoms. Adding functional groups such as NH₂ to the structure of MOFs can create and improve the hydrogen bonding between dye and MOF [69,70].

2.4. Recent Advances in Adsorptive Removal of Dyes using MOFs

MOFs, due to their excellent performances in contaminant removal from the aqueous phase, have been widely used in different wastewater treatment applications. Applying MOFs by adsorption [64] and photocatalytic degradation [70–72] has been considered in recent years for removing various pollutants such as PPCPs [73], heavy metals [74], pesticides [75], and herbicides [76] from the aquatic environment. Among these, one of the most essential applications of MOFs is adsorbing dyes from the aquatic environment. Several chemical and water-stable MOFs, such as MIL-100 [77], MIL-101 [78,79], ZIF-8 [80], UiO-66 [81], and MOF-235 [82], have been identified and applied in adsorptive removal of dyes from the aquatic environment [83,84]. These MOFs have excellent thermal and chemical stability due to the strong bonds between the metal or clusters and the ligands [85]. In addition, their high porosity leads to a high surface area, which in turn provides excellent performance in wastewater treatment applications. It can be easily washed and regenerated by acetone [86] or ethanol [87], etc., and used for successive cycles without significant performance changes. Table 2 summarizes some recent advances on dye adsorption using MOFs.

Table 2. Recent studies in adsorption of dyes using bare MOFs.

MOF	Dye	Maximum Adsorption Capacity (mg/g)	Mechanism	Thermodynamic Condition	Ref.
TMU-34	RB-B	34.58	Electrostatic, H-bonding		[71]
MIL-101(Cr)	Uranine	127	Electrostatic	Positive ΔH , ΔS Negative ΔG	[72]
MIL-100(Fe)	MB	736.2	Electrostatic	-	[73]
MIL-100(Cr)	MB	645.3	Electrostatic	-	[73]
MIL-100(Fe)	MO	1045	Electrostatic	-	[73]
MIL-100(Cr)	MO	212	Electrostatic	-	[73]
MIL-68(Al)	MB	666.7	Electrostatic, π - π	-	[74]
MIL-68(Al)	MG	153.8	Electrostatic, π - π	-	[74]
MIL-68(Al)	MO	341.3	Electrostatic, π - π	Positive ΔH , ΔS Negative ΔG	[75]
MIL-125(Ti)	RhB	59.9	-	Negative ΔH , ΔG Positive ΔS	[76]
MIL-68(In)	CR	1204	π - π	-	[77]
MIL-100(Fe)	CR	714.3	Electrostatic	Positive ΔH , ΔS Negative ΔG	[78]
MIL-100(Fe)	AO7	480.8	Electrostatic	Positive ΔH , ΔS Negative ΔG	[79]

MIL-53(Fe)	MR	183.5	Electrostatic, π - π	Negative ΔH , ΔG Positive ΔS	[80]
UiO-66	ARS	400	Electrostatic, H-bonding	-	[81]
UiO-66	MB	90	-	-	[82]
UiO-66	RhB	256	-	Positive ΔH , ΔS Negative ΔG	[83]
UiO-66	MO	83.7	Electrostatic, π - π	Negative ΔH , ΔS , ΔG	[84]
UiO-66	MB	69.8	Electrostatic	Positive ΔH , ΔS Negative ΔG	[84]
UiO-67	MG	357.3	Electrostatic, π - π	Positive ΔH , ΔS Negative ΔG	[85]
UiO-67	CR	1236.9	Electrostatic, π - π	Positive ΔH , ΔS Negative ΔG	[85]
UiO-67	MB	48.5	-	-	[85]
UiO-67	SY	47.2	-	-	[85]
UiO-67	RhB	41.3	-	-	[85]
UiO-67	MO	132.6	-	-	[85]
PCN-222	MB	906	Electrostatic, π - π	Negative ΔH , ΔG Positive ΔS	[86]
PCN-222	MO	589	Electrostatic, π - π	Negative ΔH , ΔG Positive ΔS	[86]
UiO-66	MB	145	Electrostatic, π - π	Negative ΔG	[64]
UiO-66	MO	639	Electrostatic, π - π	Negative ΔG	[64]
UiO-66	CR	827	Electrostatic, π - π	Negative ΔG	[64]
UiO-66	AC	230.9	Electrostatic, π - π	Negative ΔG	[64]
ZIF-8	Methyl blue	2500	Electrostatic	-	[87]
ZIF-67	MG	2430	π - π interac- tions	Positive ΔH , ΔS Negative ΔG	[88]
HKUST-1	MB	200	H-bonding, Electrostatic, π - π	Negative ΔH , ΔG Positive ΔS	[89]
MOF-235	MO	477	Electrostatic	Positive ΔH , ΔS Negative ΔG	[90]
MOF-235	MB	252	Electrostatic	Positive ΔH , ΔS Negative ΔG	[90]
MOF-235	LY	250	Hydrophobic, π - π	Negative ΔH , ΔG Positive ΔS	[91]
MOF-235	CR	1250	Hydrophobic, π - π	Negative ΔH , ΔS , ΔG	[91]
MOF-235	Acid Chrome Blue K	591.8	-	Positive ΔH , ΔS Negative ΔG	[92]

TMU-8	RB5	79.36	Hydrophobic, $\pi-\pi$	Negative ΔH , ΔS , ΔG	[93]
TMU-7	CR	97	-	-	[94]
Ni-BDC	Alizarin Yellow GG	621.1	Electrostatic	-	[95]
Zn-BDC	Alizarin Yellow GG	764.8	Electrostatic, $\pi-\pi$	-	[95]
Cu-BDC	Alizarin Yellow GG	710	Electrostatic, $\pi-\pi$	-	[95]
Al-based MOF	AO7	559.3	H-bonding, Electrostatic	-	[96]
Al-based MOF	AB1	332.5	H-bonding, Electrostatic	-	[96]

2.4.1. MIL-Types MOFs

Razavi et al. [71] synthesized TMU-34 for RB-B dye from the aquatic environment. TMU-34 showed fast adsorption kinetics and removed more than 90% of dye in 2 min. TMU-34 also showed an excellent adsorption performance over a mixture of dyes including MB, RB-B, and MO-RB-B due to strong host–guest interactions between RB-B and TMU-34. Tong et al. [73] utilized MIL-100(Fe) and MIL-100(Cr) to adsorb methylene blue (MB) and MO from the liquid phase. MIL-100(Fe) had a better adsorption capacity in adsorption of both dyes compared to MIL-100(Cr). The maximum capacity for MO and MB adsorption was reported to be 1045 and 736 mg/g, respectively, using MIL-100(Fe), while the maximum capacity of MIL-100(Cr) for MO and MB adsorption was 211.8 and 645.3 mg/g, respectively. A larger value of binding energy for MIL-100(Cr) with water indicates that H₂O and MO adsorption are more competitive on MIL-100(Cr). In the aquatic environment, both adsorbents have a negatively charged surface. The electrostatic attraction between MIL-structures and MB leads to excellent adsorption and high adsorption capacity. In a mixture composed of methyl orange and methylene blue, MIL-100(Cr) can remove 100% of MB and 8% MO, while MIL-100(Fe) can adsorb 100% MB and 85% MO. This study confirmed that MIL-100(Fe) could be used to simultaneously adsorb methyl orange and methylene blue, while MIL-100(Cr) is more suitable for selective removal of MB from the dye mixture, with both MIL-100(Fe) and MIL-100(Cr) being useful depending on the target application. It can also be inferred from this experiment that the central metal of MOF has had a great effect on the removal performance from the aquatic environment. Tehrani et al. [74] synthesized MIL-68(Al) to investigate the removal of MG and MB dyes from the aquatic environment. The maximum adsorption capacity of 153.8 for MG and 666.7 for MB was reached. The adsorbents were quickly regenerated with solvents such as methanol and could be reused up to three cycles with the best performance. Easy regeneration and performance maintenance are among the most important features for commercial feasibility. Wu et al. [75] working on MIL-68(Al) reached the maximum capacity of 341.3 mg/g for MO adsorption. Thermodynamic studies revealed that the processes of MO adsorption over MIL-68(Al) were endothermic, with positive entropy. The strong electrostatic and H-bonding between MO and MIL-68(Al) contributed to MO adsorption. Elsewhere, Al Sharbati et al. [97] synthesized MIL-53(Al) and explored the uptake of cationic MG and anionic MO from the water. MIL-53(Al) could quickly remove MO and MG up to 95%. MIL-53(Al) was easily regenerated through washing with ethanol and re-used for up to four cycles without any reduction in the removal efficiency, as displayed in Figure 2A. $\pi-\pi$ stacking and H-bonding were the main interactions in these experiments. Both dyes showed an endothermic adsorption onto MIL-53(Al). MIL-125(Ti) was prepared using solvothermal method by Guo et al. [76] who investigated RhB adsorption from water. The maximum capacity of RhB adsorption was 59.9 mg/g at 25 °C and pH = 7. The adsorption of RhB onto MIL-125(Ti) was spontaneous and exothermic. Jin et al. [77] synthesized

nano-rods MIL-68(In) by a solvothermal method within a short time (30 min). MIL-68(In) has a high BET surface area ($1252 \text{ m}^2/\text{g}$). MIL-68(In) showed a rapid adsorption rate and maximum capacity of 1204 mg/g in CR dye adsorption. As shown in Figure 2B, the nano-rods in MIL-68(In) have almost four times more adsorption capacity than micro-rods in MIL-68(In). The mesopore volume and larger surface area cause more adsorption capacity of nano-rods compared to micro-rods. Moradi et al. [78] synthesized MIL-100(Fe) with a high BET surface area of $2800 \text{ m}^2/\text{g}$ to remove CR from wastewater. The presence of carboxylic acid group as well as open and active metal sites suggest the excellent adsorption performance of MIL-100(Fe) over CR. An endothermic and spontaneous adsorption of CR on MIL-100(Fe) was observed. MIL-100(Fe) revealed better adsorption capacity (714.3 mg/g) compared to other common adsorbents such as chitosan/CNT (450.4 mg/g), cellulose/ Fe_3O_4 /activated carbon (66.1 mg/g), and MMT-CTAB (358 mg/g), suggesting that MIL-100(Fe) can be a proper choice in removing CR from the aquatic environment. Tsai et al. [79] prepared MIL-100(Fe) to investigate the adsorption of AO7 dye. A maximum capacity of 480.8 mg/g was obtained for the AO7 removal at 45°C . The study of thermodynamic parameters revealed the endothermic and spontaneous adsorption of AO7 on MIL-100(Fe). The electrostatic interactions between adsorbent and dye molecules constitute the main interaction in the adsorption.

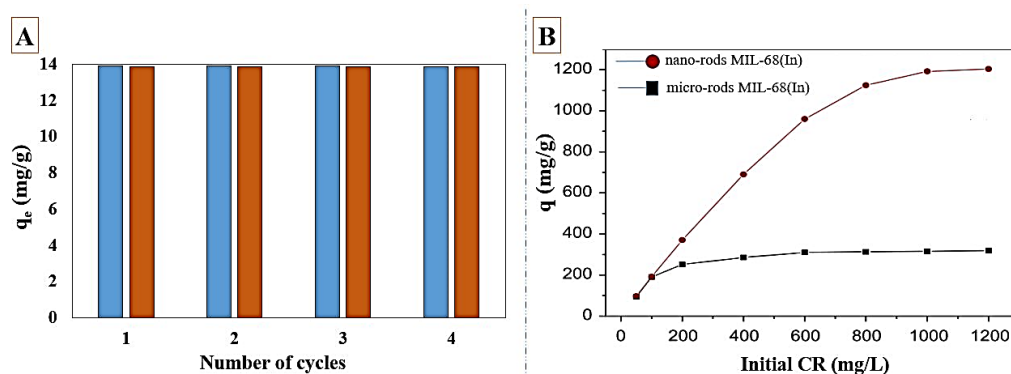


Figure 2. Effect of four cycles of regeneration on adsorption performance (A) of MIL-53(Al) over MO and MG adsorption at 298 K , $\text{pH} = 6$, contact time = 180 min, $C_0 = 13 \text{ mg/L}$; reprinted with permission from Ref. [97]. Copyright 2020 Elsevier. (B) Adsorption performance of nano-rods and micro-rods MIL-68(In) at different concentrations in 60 min; reprinted with permission from Ref. [77]. Copyright 2015 Elsevier.

To investigate the adsorption behavior of cationic MB and anionic methyl blue dyes on MIL-types MOF, Jia et al. [98] synthesized MIL-100(Fe) with a high BET surface area ($1525 \text{ m}^2/\text{g}$), and mesoporous cage. The ΔH value in adsorption of methyl blue was positive, while the ΔH value of MB adsorption onto MIL-100(Fe) was negative. According to the zeta potential results, the surface charge of adsorbent was negative within the pH range of 1–10 and MIL-100(Fe), where a negatively charged surface may show better adsorption performance over positively charged surface pollutants. That may explain why MIL-100(Fe) showed better adsorption efficiency over cationic MB (about 100%) compared to anionic methyl blue (52.1%). Yilmaz et al. [80] prepared MIL-53(Fe) for examining the adsorption of MR dye from the aqueous phase. Based on the kinetic study, MR adsorption onto MIL-53(Fe) obeyed the pseudo-second-order kinetic model. As reported in Table 3, MIL-53(Fe), with a minimal BET surface area, has had a better performance for MR capture from the aquatic environment than modified zeolite and activated carbon [99,100].

Table 3. Performance of various adsorbents over MR adsorption from the aquatic environment; reprinted with permission from Ref. [80]. Copyright 2016 Elsevier.

Adsorbent	BET Surface Area (m ² /g)	q _{max} (mg/g)
MIL-53 (Fe)	23	183.5
Commercial activated charcoal	-	30
Modified zeolite	-	7
Activated carbon	-	40.5

2.4.2. Zirconium-Based MOFs

Zirconium-based MOFs cover a wide range of MOFs including UiO-series such as UiO-66 [101], UiO-67 [102], and UiO-68 [103], as well as PCN-series such as PCN-222 [104], PCN-521 [105], MOF-808 [106], MOF-812 [107], NU-1000 [108], and NU-1100 [109]. Zr-based MOFs have efficient performance in the removal of various contaminants from the aquatic environment, especially dyed contaminants. They are widely used in water treatment applications [110].

Embaby et al. [81] synthesized UiO-66 via microwave-assisted method. All experiments were carried out at 25 °C, shaking at 200 rpm for 2 h. According to Table 4, UiO-66 showed a better adsorption performance over anionic dyes, while the removal of cationic dyes was very low and negligible. Anion exchange of the Zr₆O₄(OH)₄ nodes of UiO-66 with anionic adsorbates as an adsorption mechanism would lead to better removal efficiency of anionic dyes over UiO-66. On the other hand, hydrogen bonding between SO₃⁻ and -OH on the UiO-66 nodes would result in the anionic dyes being attracted to the MOF and better adsorbed onto the MOF surface.

Table 4. Performance of UiO-66 in the removal of cationic vs. anionic dyes; reprinted with permission from Ref. [81]. Copyright 2018 Elsevier.

Cationic Dyes	Removal (%)	Anionic Dyes	Removal (%)
Neutral red (NR)	3.4	Alizarin red S (ARS)	81
Methylene blue	4.43	Eosin (E)	80
Fuchsin basic (FB)	0.98	Fuchsin acid (FA)	40
Safranin T (ST)	3.41	Methyl orange (MO)	31

As displayed in Figure 3A, the positively charged surface of UiO-66 has stronger electrostatic interactions with anionic dyes. Mohammadi et al. [82] synthesized UiO-66 with crystalline sizes of 153–213 nm, and a surface area of 765 m²/g to investigate MB adsorption from water. The maximum adsorption (90 mg/g) was reached at pH = 9. The zeta potential was 6, where the negatively charged surface of UiO-66 at the pH ranges above 6 was more favorable for adsorption for cationic MB dye. To investigate the removal of RhB dye from the aquatic environment, He et al. [83] synthesized UiO-66 with a BET surface area of 486.4 m²/g, and an average pore diameter of 4.85 nm. The maximum capacity of 135–256 mg/g was obtained at 0–50 °C for the RhB adsorption. The adsorption of RhB on UiO-66 was endothermic, and higher temperatures were more favorable for the processes. In addition to relatively good adsorption capacity, the regenerated UiO-66 revealed an excellent performance in experiments up to seven cycles as shown in Figure 3B. Molavi et al. [84] reported the synthesis of UiO-66 and employed it in the adsorption of MB plus MO from wastewater. Electrostatic interactions between anionic MO and UiO-66 in neutral and acidic environments would lead to higher capacity of MO adsorption (83.7 mg/g) than MB adsorption (69.8 mg/g). In this study, the long-term water stability of synthesized UiO-66 was confirmed for one year. Examination of the XRD pattern of the UiO-66 after 12 months of presence in water did not show much change in diffraction patterns, suggesting that the synthesized UiO-66 structure was maintained in the aqueous environment even after a very long time. UiO-66 placed in the aquatic environment for 1

year was able to adsorb MO with 70% of the initial capacity. This reduction in MO uptake was related to the reduction in the surface area from 1276 to 972 m²/g during 12 months. Figure 3C presents the performance of UiO-66 placed in water after 3, 9, and 12 months in MO and MB adsorption. Another Zr-based MOF, UiO-67, was synthesized by Yang et al. [85] and applied in adsorption of MG and CR from the aquatic environment. The maximum capacity of 357.3 and 1236.9 mg/g was reported for the MG and CR adsorption, respectively. Great affinity of SO₃⁻ group of CR and Zr-OH groups of UiO-67 would result in the high adsorption capacity of CR. The π - π interactions between aromatic compounds of both dyes and UiO-67 and electrostatic interactions were other major interactions in the adsorption of MG and CR over UiO-67. In addition to CR, the adsorption of MB, SY, RhB, and MO was also examined in this study. The maximum capacity of MB, SY, RhB, and MO adsorption was 48.5, 47.2, 41.3, and 132.6 mg/g, respectively, under the same conditions.

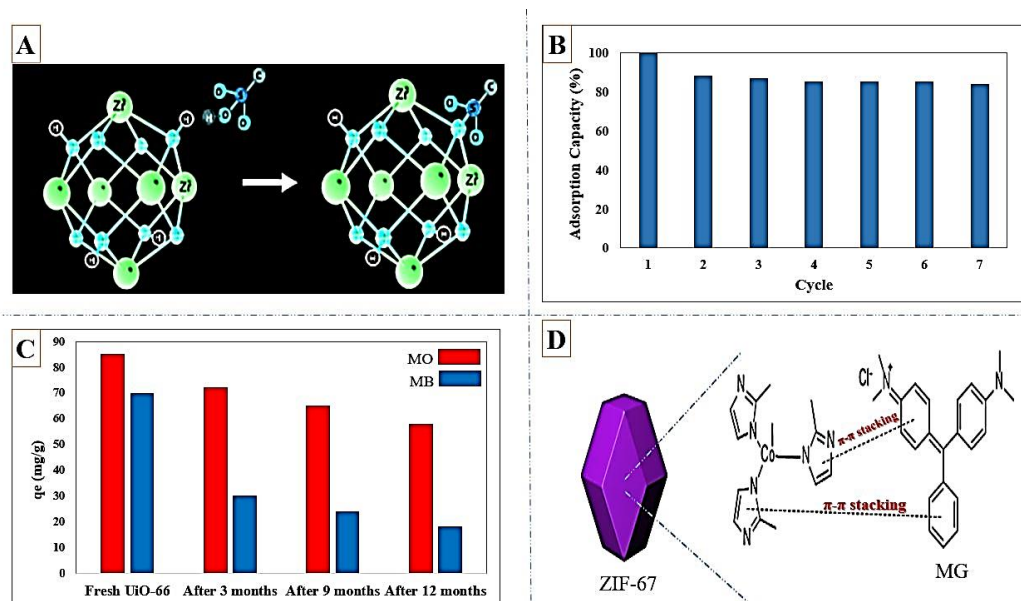


Figure 3. Anionic (A) SO₃⁻ group interacting with Zr₆O₄(OH)₄ nodes of UiO-66; reprinted with permission from Ref. [81]. Copyright 2018 Elsevier. (B) Regenerated performance of UiO-66 in RhB adsorption up to seven cycles; reprinted with permission from Ref. [83]. Copyright 2014 Elsevier. Fresh and stored in the aquatic environment after 3, 9, and 12 months (C) performance of UiO-66 in MO and MB adsorption; reprinted with permission from Ref. [84]. Copyright 2018 Elsevier. (D) The primary mechanism of MG adsorption from water by ZIF-67; reprinted with permission from Ref. [88]. Copyright 2015 Elsevier.

Li et al. [86] synthesized PCN-222 with a BET surface area of 2336 m²/g under solvothermal condition and utilized it in the removal of MB and MO from the aquatic environment. PCN-222 indicated an excellent adsorption performance toward dyes, with a maximum capacity of 906 and 589 mg/g for the MB and MO adsorption, respectively. This Zr-based MOF also showed excellent performance in adsorption from a mixture containing MO and MB, with the ability to adsorb 1239 and 1022 mg/g, respectively. The adsorption processes were exothermic and spontaneous. In addition to the excellent adsorption capacity, PCN-222 could also be regenerated and reused up to several successive cycles, where the removal efficiency diminished to 92.7% for MO and to 95.2% for MB after eight cycles.

2.4.3. Zeolitic Imidazolate Frameworks (ZIFs)

Zeolitic Imidazolate Frameworks (ZIFs) are composed of imidazolate linkers and metal ions with a structure similar to aluminosilicate zeolites [111]. ZIFs enjoy both the

structural properties of zeolites and MOFs, conferring them a high surface area, high crystallinity, and unimodal micropores [112,113].

ZIF-8 [87] and ZIF-67 [88] are the most important structures used in the adsorption of dyed pollutants from the aquatic environment. Feng et al. [87] synthesized ZIF-8 and utilized it in removing methyl blue from the water. ZIF-8 revealed an excellent adsorption capacity of 2500 mg/g. The sorption saturation occurred within less than 45 min and the adsorption rate was very fast. The strong ionic bonding between negatively charged SO_3^- groups in methyl blue and positively charged Zn^{2+} in ZIF-8 contributed to improving the adsorption performance. In this study, the removal of MB, MO, and RhB was also investigated by ZIF-8, where the adsorption capacity of 18, 20, and 40 mg/g was reported for MO, MB, and RhB, respectively. The higher adsorption capacity of methyl blue compared to the other three dyes indicates the higher selectivity of adsorption methyl blue onto ZIF-8. Lin et al. [88] synthesized a high-stable ZIF-67 for the MG dye adsorption from the aquatic environment. ZIF-67 presented an excellent maximum capacity of 2500 mg/g at 20 °C and 2941 mg/g at 40 °C, which were higher than the values of other common adsorbents. Table 5 compares the adsorption capacity of MG over ZIF-67 and other adsorbents. ZIF-67 also exhibited a high regeneration efficiency and maintained the removal efficiency of more than 95% up to four cycles. Investigation of thermodynamic parameters revealed an endothermic and spontaneous adsorption. As depicted in Figure 3D, π - π stacking between aromatic compounds of MG and imidazole rings on ZIF-67 was the primary interaction for the MG adsorption in this study.

Table 5. Performance of various adsorbents in MG adsorption from the aquatic environment compared to ZIF-67; reprinted with permission from Ref. [88]. Copyright 2015 Elsevier.

Adsorbent	T (°C)	Adsorption Capacity (mg/g)
Cyclodextrin-based material	25	92
Coconut shell-based AC ¹	60	214
Bamboo-based AC	30	263
Commercial AC	30	222
Oxalic-acid-modified sawdust	60	280
Chitosan beads	30	93
ZIF-67	20	2500
ZIF-67	40	2941
ZIF-67	60	3226

¹ AC means Activated Carbon.

Santoso et al. [114] synthesized ZIF-8 with acetic acid, ZIF-8(AA), for adsorption of MB from the aquatic environment. In this study, the structural characteristics and the performance in MB uptake of ZIF-8(AA) were compared against ZIF-8 synthesized with DMF solvent, ZIF-8(DMF). ZIF-8(DMF) had a higher BET surface area (1013 to 538 m²/g) and higher crystallinity (100% to 32.75%) compared to ZIF-8(AA). The particle size of ZIF-8(AA) was 62.5 nm, while the particle size of ZIF-8(DMF) was 2500 nm. The adsorption experiments revealed a better performance of ZIF-8(AA) with almost 50% the surface area compared to ZIF-8(DMF). The better adsorption performance of ZIF-8(AA) than ZIF-8(DMF), despite the smaller surface area, was due to the higher mesoporosity of ZIF-8(AA). In addition, the presence of oxygen atoms in the acetate on the ZIF-8(AA) and its affinity toward MB would support a better performance in adsorption.

2.4.4. Other Types of MOFs

Lin et al. [89] synthesized Cu-based MOF, HKUST-1, also known as Cu-BTC, for removing MB from the aquatic phase. The maximum capacity obtained for MB adsorption was 200 mg/g, at pH = 7. Thermodynamic parameters indicated an exothermic and spon-

taneous adsorption of MB on HKUST-1. H-bonding and π - π stacking between the aromatic compounds of MB and HKUST-1 were the primary adsorption interactions in this experiment.

MOF-235 as a Fe-based MOF has presented an adequate performance in absorbing anionic and cationic dyes [115,116]. MOF-235 synthesized by Haque et al. [90] showed an adsorption capacity of 252 mg/g for MB and 477 mg/g for MO. In this experiment, MOF-235 failed to adsorb nitrogen from the aqueous phase, while presenting an excellent performance in adsorptive removal of dyes. It can be concluded that MOF-type adsorbents can offer good performance in removing dyes from the aquatic environment even if they cannot adsorb gases from the aqueous phase.

Dou et al. [91] synthesized MOF-235 to adsorb lemon yellow (LY) and CR dyes from water. The strong π - π and hydrophobic interactions between MOF-235 and CR and LY would result in an excellent adsorption performance of MOF-235 with a maximum capacity of 250 and 1250 mg/g for LY and CR adsorption, respectively. The adsorbent utilized in this experiment was quickly recovered and regenerated with ethanol and sodium hydroxide solution and applied for up to six cycles without significant change in the performance. Indeed, the adsorption capacity of CR and LY obtained was 1027 and 213 mg/g, respectively, after six cycles. Ge et al. [92] synthesized MOF-235 via a microwave-assisted thermolysis method to the adsorption of Acid Chrome Blue K from the water. The maximum capacity obtained for the Acid Chrome Blue K adsorption was 591.8 mg/g at 20 °C. Due to MOF-235 high adsorption capacity and fast performance in Acid Chrome Blue K uptake from the aquatic environment, the application of MOF-235 was confirmed in this study as an efficient adsorbent in dyed-contaminants wastewater.

Hazrati et al. [93] synthesized TMU-8 with the solvothermal method and applied it to remove reactive black 5 (RB5) dye from the aquatic environment. The maximum capacity obtained was 79.36 mg/g for the RB5 adsorption. Formation of the π - π interactions between dye and TMU-8 ligand, along with the hydrophobic interaction were the main interactions in RB5 adsorption by TMU-8. To investigate the CR dye adsorption and to compare the dye removal performance of two adsorbents synthesized by the sonochemical and the mechanochemical method, Masoomi et al. [94] synthesized TMU-7. As shown in Figure 4A, the adsorbents obtained from sonochemical method revealed a faster adsorption performance in CR uptake. The maximum capacity of sonochemically synthesized TMU-7 obtained was 97 mg/g for the CR adsorption. To explore the effect of central metals on the adsorptive removal of Alizarin Yellow GG from the aquatic environment, Liu et al. [95] synthesized three two-dimensional MOFs, including Ni-BDC, Cu-BDC, and Zn-BDC. The BET surface area obtained was 4.60, 14.41, and 15.07 m²/g for Ni-BDC, Cu-BDC, and Zn-BDC, respectively. Different morphologies such as peony-like, rectangle sheet, and irregular sheet were obtained using different central metal ions in Ni-BDC, Cu-BDC, and Zn-BDC, respectively. The maximum capacity of Alizarin Yellow GG adsorption over MOFs obtained was 621.1, 710, and 764.8 mg/g for Ni-BDC, Cu-BDC, and Zn-BDC, respectively. The performance of these three MOFs at different temperatures is shown in Figure 4B. Adsorption capacities indicated more affinity between anionic Alizarin Yellow GG dye and Zn-BDC as well as Cu-BDC compared to Ni-BDC, well suggesting the role of the central metal ion of MOF in adsorption performance. π - π stacking and H-bonding were the main interactions in the Alizarin Yellow GG adsorption by these MOFs. As outlined in Table 6, all three synthesized MOFs far outperformed other adsorbents in adsorption of Alizarin Yellow GG dye.

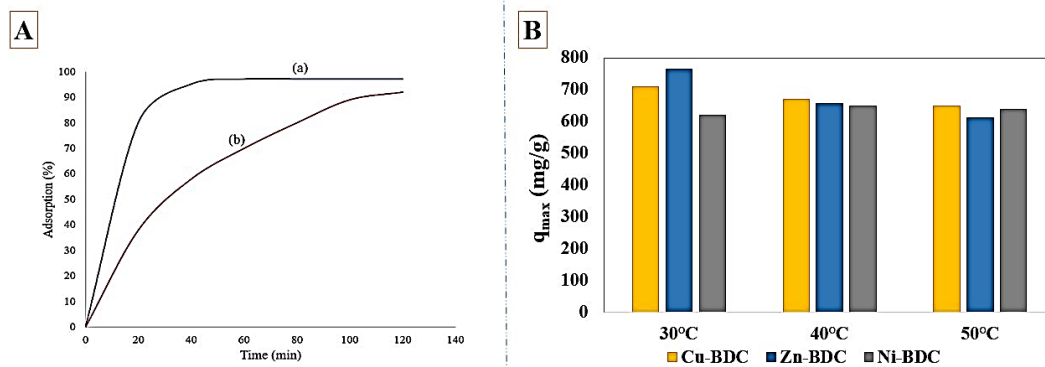


Figure 4. (A) The sonochemically synthesized (a) TMU-7 and mechanochemically synthesized (b) TMU-7 performance in CR adsorption from the aquatic environment; reprinted with permission from Ref. [94]. (B) The maximum adsorption capacity of Cu-BDC, Zn-BDC, and Ni-BDC in Alizarin Yellow GG uptake from water; reprinted with permission from Ref. [95].

Table 6. Adsorption capacity of Cu-BDC, Ni-BDC, and Zn-BDC compared to other adsorbents; reprinted with permission from Ref. [95]. Copyright 2020 Elsevier.

Adsorbent	Adsorption Capacity (mg/g)
Cu-BDC	710
Ni-BDC	621.1
Zn-BDC	764.8
Ar@MCM	400
Modified polymer	15.9
Fe ₃ O ₄ @MCM@Cu-Fe-LDH	121.9
nZVI/PANI/APT	72
DNPH- γ -Alumina	47.8
γ -Alumina	37.7

3. Optimized MOF

Efforts are made to improve the structural properties of adsorbents through modification or development of composites for more efficient performance in wastewater treatment applications. Structural modification of adsorbents leads to more favorable conditions such as higher stability in the aquatic or acid–basic environments [117], easy recovery [118], and better adsorption capacity [119]. Despite the unique properties of MOFs, some weaknesses of their structure, such as restricted absorption capacity and low stability in aquatic environments, limit their use in water treatments. Several optimization methods have been considered to address these restrictions and improve the properties. Adding modified groups to the organic ligands [120], adjusting pore size and pore structure of MOFs with different ligands, changing the synthesis method [121], or combining MOF with nanoparticles to fabricate an MOF-based nanomaterial have been proposed for improving the adsorption performance of MOFs [122]. In this study, the primary purpose is on MOF-based composites with improved structural properties compared to bare MOFs.

3.1. Magnetic MOFs

MOF-based magnetic composites composed of a magnetic nanoparticle and a metal–organic framework have recently received attention for catalysis [123], drug delivery [124], and water purification [125]. The introduction of magnetic nanoparticles into the MOFs structure leads to rapid and easy recovery by applying an external magnetic field in various applications [126]. Different methods are used to integrate magnetic nanoparticles into the MOFs, such as layer-by-layer growth of MOFs on magnetic nanoparticles

[127–129], encapsulation of magnetic particles into MOFs [130,131], and sedimentation of magnetic nanoparticles on the MOFs' structure by a solvothermal method [127,132,133]. High specific surface area and low toxicity of Fe₃O₄ nanoparticles result in widespread use of these particles for magnetized MOFs. Porous MOFs can be used to encapsulate magnetic nanoparticles. The incorporation of magnetic nanoparticles onto MOFs reduces the pore volume of the composite and BET surface area, while sparing the pore size distribution of the MOFs matrix [134]. Several MOFs such as MIL-100 [135], ZIF-8 [136], UiO-66 [137], and MIL-101 [138] are utilized to encapsulate magnetic nanoparticles. Recent advances in dye removal by magnetic MOF are reported in Table 7.

Table 7. Recent advances in dye removal using magnetic MOF.

MOF	Dye	Maximum Adsorption Capacity (mg/g)	Mechanism	Thermodynamic Condition	Ref.
Fe ₃ O ₄ /MIL-100(Fe)	RhB	28.36	Electrostatic, π - π	Positive ΔH and ΔS	[139]
ZIF-8@SiO ₂ @MnFe ₂ O ₄	MG	1010.2	Electrostatic, π - π	-	[140]
ZIF-8@SiO ₂ @MnFe ₂ O ₄	MO	78.1	Electrostatic	-	[140]
Fe ₃ O ₄ /MIL-101(Cr)	AR1	142.9	Electrostatic	Negative ΔH , ΔS , ΔG	[141]
Fe ₃ O ₄ /MIL-101(Cr)	Orange G	200	Electrostatic	Negative ΔH , ΔS , ΔG	[141]
Cu-MOF/Fe ₃ O ₄	MG	113.7	-	Positive ΔH , ΔS Negative ΔG	[142]
Fe ₃ O ₄ /HKUST-1	MB	2.96	Electrostatic	Positive ΔH , ΔS Negative ΔG	[143]
Fe ₃ O ₄ /MIL-101(Cr)	FS	78	Electrostatic	-	[144]
Fe ₃ O ₄ /MIL-101(Cr)	XO	98	Electrostatic	-	[144]
Fe ₃ O ₄ /MIL-101(Cr)	MO	79	Electrostatic,	-	[144]
Fe ₃ O ₄ /HKUST-1	MB	245	π - π , Hydrophobic	-	[145]
Fe ₃ O ₄ -ZTB-1	CR	458	Electrostatic, H-bonding	-	[146]

Magnetic MOFs in Dye Removal

Liu et al. [139] synthesized magnetic MIL-100(Fe) for the removal of RhB dye from the aquatic environment. The adsorbent showed an excellent performance and can be reused for up to five cycles without any significant change in performance.

Abdi et al. [140] synthesized ZIF-8@SiO₂@MnFe₂O₄ as a magnetic MOFs with a maximum uptake capacity of 1010.2 and 78.12 mg/g for MG and MO, respectively. MnFe₂O₄ nanoparticle was synthesized through coprecipitation method in this study. In this method, the metal was precipitated in the form of hydroxide with the help of a base solution in a solvent. The SiO₂ particles were prepared by Stöber method. π - π interaction between imidazole rings in the MOF structure with the aromatic rings of MG dye molecules would cause more efficient adsorption of MG from the aquatic environment. Wang et al. [141] reported the synthesis of Fe₃O₄/MIL-101(Cr) based on a reduction-precipitation technique. The maximum capacity obtained was 142.9 mg/g for AR1 and 200 mg/g for the orange G adsorption. This magnetic MOF can easily be separated with an external magnetic field such as magnet, and regenerated and reused up to six times. As displayed in Figure 5A,B, despite the lower surface area of Fe₃O₄/MIL-101(Cr) than MIL-101(Cr), and the reduction in the surface area from 3312 m²/g to 1482 m²/g by magnetizing MIL-101(Cr), the magnetic composite even outperformed MIL-101(Cr) in some cases. Magnetic Fe₃O₄/MIL-101(Cr), in addition to presenting almost the identical dye removal perfor-

mance, has also the advantage of separability from the adsorption environment by a magnetic field. Shi et al. [142] synthesized Cu-MOF/Fe₃O₄, to remove MG dye from the aquatic environment. The maximum adsorption capacity was found to be 113.7 mg/g. Matched molecular size of the MG dye and MOF pore sizes of Cu-MOF/Fe₃O₄ was the main reason for the excellent performance of the magnetic composite in MG removal from the aquatic environment, where dye molecules would easily enter the MOF cavities and be adsorbed. The adsorption of MG on magnetic composite was endothermic, and spontaneous. Xu et al. [143] synthesized a Cu-based MOF, HKUST-1, and Fe₃O₄/HKUST-1 magnetic composite. In this study, the magnetic Fe₃O₄ particles were prepared via one-pot hydrothermal technique where the synthesized Fe₃O₄-embedded-MOF was used to remove MB dye from the aquatic environment. The removal efficiency was about 70%, with a maximum capacity of 2.96 mg/g for the MB adsorption. Magnetizing HKUST-1 reduced its BET surface area from 1316 to 939, which was due to the presence of Fe₃O₄ particles within HKUST-1 structure and space occupation. Jiang et al. [144] synthesized Fe₃O₄/MIL-101(Cr) with a high BET surface area of 3300 m²/g and applied it to remove XO, FS, and MO from the aquatic environment. As illustrated in Figure 5C, the electrostatic interactions between adsorbent and anionic dyes would lead to a better adsorption performance. Fe₃O₄/MIL-101(Cr) with the possibility of easy recovery from the adsorption environment and excellent performance up to five cycles after regeneration proved to a suitable option in wastewater treatment. Zhao et al. [145] synthesized magnetic Cu-BTC, also known as HKUST-1, through incorporating Fe₃O₄ particles onto HKUST-1 for removing MB dye from the aquatic environment. Hydrophobic and π - π interactions between MB dye and magnetic composite were the main adsorption mechanism in this study. The adsorption of MB over Fe₃O₄/HKUST-1 was endothermic and spontaneous. Han et al. [146] synthesized highly water-stable magnetic ZTB-1 to remove CR from water. The strong electrostatic interactions and H-bonding between -NH₂ groups of CR dye and C=O bond of Fe₃O₄-ZTB-1 led to an excellent adsorption performance and high adsorption capacity in CR uptake.

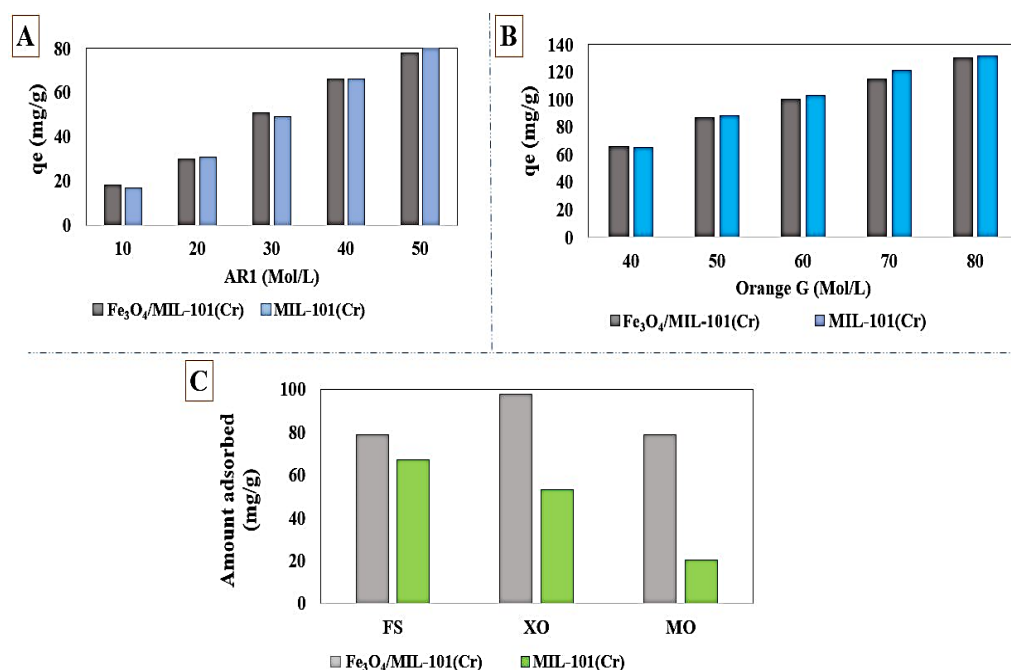
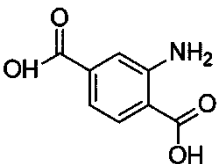
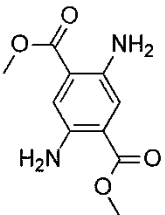
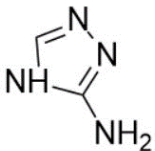
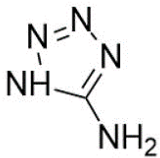
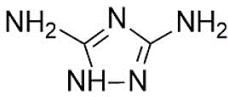


Figure 5. The performance of Fe₃O₄/MIL-101(Cr) in removing (A) Acid Red1 and (B) Orange G, reprinted with permission from Ref. [141]. Copyright 2016 Elsevier. (C) The amount adsorbed of FS, XO, and MO on Fe₃O₄/MIL-101(Cr); reprinted with permission from Ref. [144]. Copyright 2016 Elsevier.

3.2. Amine-Functionalized MOFs

Introducing amine functional groups to the metal–organic frameworks referred to as amine-functionalized MOFs has attracted attention to optimize the adsorption performance of MOFs in aquatic environments. Amine-functionalized metal–organic frameworks are used to adsorb various anionic and cationic dyes. The emergence of new interactions such as hydrogen bonding and steric hindrance as well as regulation of surface charge distribution improve the adsorption process. These composites are prepared via three main methods, including physical mixing amines and MOFs [147], in situ synthesis [148,149], and post-modification with polyamines. Adding amine compounds such as $-NH_2$ to the MOF structure or using amine-ligands in the synthesis are the basis for the amine-functionalized MOF preparation. Some of the most widely used organic amine-linkers are listed in Table 8.

Table 8. The reported amine-linkers and their structure information.

Ligands	Molecular Mass (g/mol)	Molecular Formula	Chemical Structure	Ref
2-Aminoterephthalic acid	181.5	$C_8H_7NO_4$		[150]
Dimethyl 2,5-diaminobenzene-1,4-dicarboxylate	224.2	$C_{10}H_{12}N_2O_4$		[151]
3-amino-1,2,4-triazole	84.1	$C_2H_4N_4$		[152]
5-Aminotetrazole	85.1	CH_3N_5		[153]
3,5-diamino-1,2,4-triazole	99.1	$C_2H_5N_5$		[154]

Due to a facile synthesis route, structural stability in the solvent, and a high adsorption capacity, amino-functionalized MOFs can be considered promising adsorbents in aqueous solutions. Electrostatic interaction between amine groups in MOFs structure with dye molecules would enhance the adsorption capacity. Recent advances in dye removal by amine-functionalized MOF are presented in Table 9.

Table 9. Recent advances in dye removal using amine-functionalized MOF.

MOF	Dye	Maximum Adsorption Capacity (mg/g)	Mechanism	Thermodynamic Condition	Ref.
NH ₂ -MIL-101(Al)	MG	274.4	Electrostatic, π - π , Hydrophobic, H-bonding	Positive ΔH , ΔS Negative ΔG	[155]
NH ₂ -MIL-101(Al)	IC	135	Electrostatic, π - π , Hydrophobic, H-bonding	Positive ΔH , ΔS Negative ΔG	[155]
NH ₂ -MIL-101(Cr)	MO	461.7	Electrostatic, π - π	-	[156]
NH ₂ -MIL-101(Cr)	Acid chrome blue K	259.8	Electrostatic, π - π	-	[156]
NH ₂ -MIL-101(Cr)	CR	2967.1	Electrostatic, π - π , H-bonding	-	[156]
NH ₂ -MIL-125(Ti)	MB	405.6	Electrostatic	Positive ΔH , ΔS Negative ΔG	[157]
Fe ₃ O ₄ /MIL-101(Al _{0.9} Fe _{0.1})/NH ₂	MO	355.8	Electrostatic	Negative ΔH , ΔS , ΔG	[158]
NH ₂ -MIL-101(Al)	MB	762	Electrostatic	Positive ΔH , ΔS Negative $\Delta G < 0$	[120]
NH ₂ -MIL-101(Al)	MO	188	-	Positive ΔH , ΔS Negative ΔG	[120]
NH ₂ -MIL-101(Al)	MG	274.4	Electrostatic, π - π , H-bonding	Positive ΔH , ΔS Negative ΔG	[155]
NH ₂ -MIL-101(Al)	IC	135	Electrostatic, π - π , H-bonding	Positive ΔH , ΔS Negative ΔG	[155]
Fe ₃ O ₄ @NH ₂ -MIL-101(Cr)	MB	370.3	Electrostatic, π - π	Positive ΔH , ΔS Negative ΔG	[159]
NH ₂ -MIL-125(Ti)	MB	862	Electrostatic, π - π , H-bonding	Positive ΔH , ΔS Negative ΔG	[115]
NH ₂ -MIL-125(Ti)	BB41	1257	Electrostatic, π - π , H-bonding	Positive ΔH , ΔS Negative ΔG	[115]
NH ₂ -MIL-125(Ti)	BR46	1296	Electrostatic, π - π , H-bonding	Positive ΔH , ΔS Negative ΔG	[115]
NH ₂ -UiO-66	Safranin	390	Electrostatic	-	[160]

Amine-Functionalized MOFs in Dye Removal

Magnetic NH₂-MIL-101(Al) was synthesized by Liu et al. [155] to explore adsorption of IC and MG dyes. The maximum capacity for MG and IC adsorption was 274.4 and 135 mg/g, respectively. The greater adsorption capacity of NH₂-MIL-101(Al) compared to MIL-101(Al) was associated to the electrostatic and π - π interaction between amine groups and dye molecules. Moreover, H-bonding between the -NH₂ in adsorbent structure and dye molecules would enhance the adsorption capacity. The MG and IC adsorption onto this composite was endothermic and spontaneous at 298, 308, and 318 K. For adsorption of MO, acid chrome blue k, and CR from the water, NH₂-MIL-101(Cr) were synthesized by Zhang et al. [156]. This amine functionalized MOF revealed an excellent performance with a capacity of 461.7, 259.8, and 2967.1 mg/g for MO, acid chrome blue k, and CR adsorption, respectively. Moreover, the maximum adsorption capacity of unfunctionalized MIL-101(Cr) toward MO, acid chrome blue k, and CR obtained was 228, 217, and 1367 mg/g, respectively. As shown in Figure 6A, high adsorption of CR is attributed to the

presence of many aromatic rings in the CR structure, which leads to π - π interaction and H-bonding with NH₂-MIL-101.

In another study, Bibi et al. [157] synthesized NH₂-MIL-125 via hydrothermal method to investigate adsorption of MB dye from the aqueous media. The results indicated that the NH₂-MIL-125 had a higher surface area (1028 m²/g) compared with MIL-125 (470 m²/g). Moreover, NH₂-functionalization enhanced the adsorption performance of MIL-125 and resulted in higher adsorption capacity from 321.39 to 405.61 mg/g for MB dye. The strong electrostatic interaction between NH₂-MIL-125 and the amino groups of dye has significantly boosted the adsorption performance of the composite. An endothermic and spontaneous adsorption of MB onto NH₂-MIL-125(Ti) was reported in this study. NH₂-MIL-125(Ti) also presented excellent reusability and efficiently adsorbed MB up to four cycles.

Bao et al. [158] synthesized Fe₃O₄/MIL-101(Al_{0.9}Fe_{0.1})/NH₂, and reported a maximum capacity of 355.8 mg/g for MO adsorption. The use of two central metal ions in the MOF structure increases the water-stability of MOF and improves the adsorption performance of the composite due to the strong interactions between the central metal ions, linkers, and MO dye. To investigate the removal of MB and MO from the aquatic environment, Haque et al. [120] synthesized NH₂-MIL-101(Al) with an adsorption capacity of 762 and 188 mg/g for MB and MO at 303 K, respectively. The amino-functionalized MIL-101 outperformed non-amino-functionalized MIL-101 regarding adsorption, such that in the case of MB, the adsorption capacity of MIL-101(Al) obtained was only 195 mg/g. The strong electrostatic attractions between NH₂-MIL-101 and dye molecules would lead to better adsorption performance of amino-functionalized MIL-101 compared to non-amino-functionalized MIL-101. The adsorption of both dyes onto NH₂-MIL-101 was endothermic and spontaneous. Haochi et al. [155] synthesized Fe₃O₄@NH₂-MIL-101(Al) to remove of MG and IC. The maximum adsorption capacity obtained was 135 and 274.4 mg/g for IC and MG, respectively. In addition to the excellent adsorption performance in both IC and MG uptake from water, the easy separation from the aqueous solution, as well as good regeneration and reusability for up to five cycles were other characteristics of the synthesized magnetic NH₂-MIL-101(Al) in this study.

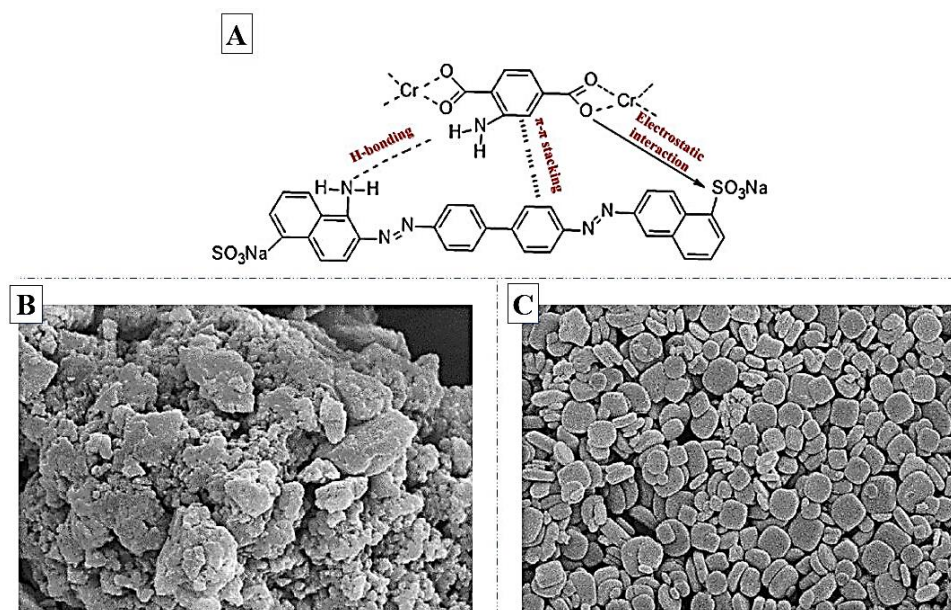


Figure 6. (A) Possible interactions between NH₂-MIL-101(Cr) and CR dye; reprinted with permission from Ref. [156]. Copyright 2020 Elsevier. The SEM images of (B) MIL-125(Ti) and (C) NH₂-MIL-125(Ti); reprinted with permission from Ref. [160]. Copyright 2018 Elsevier.

Elsewhere, Karimi et al. [159] synthesized magnetic NH₂-MIL-101(Cr) to explore the removal of MB from the aquatic environment. The maximum adsorption capacity obtained was 370.3 mg/g. The adsorption of MB on the composite was endothermic, with an increase in irregularities. Oveisi et al. [115] synthesized MIL-125(Ti) and NH₂-MIL-125(Ti) to examine the adsorption of BR46, BB41, and MB and from the aquatic environment. The SEM images of MIL-125(Ti) and NH₂-MIL-125(Ti) are presented in Figure 6B,C. Amine-functionalized MIL-125 has a BET surface area of 1350 m²/g, higher than non-functionalized MIL-125(Ti) (499 m²/g). As reported in Table 10, the higher removal efficiency of amine-functionalized MIL-125(Ti) is related to the π - π interactions between NH₂-MIL-125 and dye molecules. In addition, the hydrogen bonding between the N atom in the functional group of MIL-125 and dye molecules as another vital interaction results in better performance of NH₂-MIL-125(Ti) in dye adsorption. The adsorption of three cationic dyes onto NH₂-MIL-125(Ti) was endothermic and spontaneous. The maximum capacities of 862, 1257, and 1296 mg/g were obtained in this study for MB, BB41, and BR46 adsorption, respectively. Tambat et al. [160] synthesized NH₂-UiO-66 for investigating safranin dye removal from the aquatic environment. Strong electrostatic interactions between the dye and amine-functionalized MOF resulted in an adsorption capacity of 390 mg/g. Amine-functionalized UiO-66 presented good regeneration efficiency, and after three cycles, the adsorbent had still good performance in safranin uptake from the water.

Table 10. Dye removal efficiency of MIL-125(Ti) and NH₂-MIL-125(Ti). reprinted with permission from Ref. [115].

Adsorbent	MB Removal (%)	BB41 Removal (%)	BR46 Removal (%)
MIL-125(Ti)	39	41	45
NH ₂ -MIL-125(Ti)	97	93	99

3.3. GO- and CNT-MOF Nanocomposites

The utilization of carbon-based materials in wastewater treatment has a long history and has always been of interest. Graphene oxide (GO) is a 2-D carbon nanostructure with many oxygen functional groups such as hydroxyl, epoxy, and carboxyl. GO can be easily dispersed in polar solvents such as water [161] and can be utilized as an adsorbent in aqueous solutions. Oxygen functional groups in graphene oxide and metal nodes of MOFs form MOF/GO nanostructure, with an enhanced adsorption capacity and an improved performance for dye removal [162–166]. The structural analysis showed that in an MOF/GO nanostructure, GO thin layer and MOF particles can act as a divider and a filler. In this regard, carbon nanotubes (CNT) are carbon cylinders with a wall diameter of nanometers. These pipes are single-walled or multi-walled and have closed or open ends [167,168].

GO- and CNT-MOF Nanocomposites in Dye Removal

Since CNT [169] and GO [170] have been considered efficient adsorbents in wastewater treatment applications, MOF can be attached to CNT and GO and offer the characteristics of both carbon material and MOF with superior performance as an adsorbent. Recent advances in dye removal by MOF nanocomposites based on CNT and GO are presented in Table 11.

Table 11. Recent advances in dye removal using MOF nanocomposites based on CNT and GO.

MOF	Dye	Maximum Adsorption Capacity (mg/g)	Mechanism	Thermodynamic Condition	Ref.
GO/Cu-MOF	MB	173	π - π , Electrostatic, H-bonding	-	[171]
ZIF-8	MG	1667	π - π , Electrostatic	Positive ΔH , ΔS	[172]

					Negative ΔG	
GO/ZIF-8	MG	3300	π - π , Electrostatic	Positive ΔH , ΔS Negative ΔG	[172]	
CNT/ZIF-8	MG	2034	π - π , Electrostatic	Positive ΔH , ΔS Negative ΔG	[172]	
GO/Ni-MOF	CR	2489	Electrostatic	Positive ΔH , ΔS Negative ΔG	[173]	
GO@MOF-5	RhB	151.62	π - π , Electrostatic, H-bonding		[174]	
GO/MIL-68(Al)	MO	400	π - π , Electrostatic, H-bonding	-	[175]	
MIL-100(Fe)	MO	667	-	-	[176]	
MIL-100(Fe)	MB	1019	-	-	[176]	
GO/MIL-100(Fe)	MO	1189	-	-	[176]	
GO/MIL-100(Fe)	MB	1231	-	-	[176]	
UiO-66	AO7	42.6	-	-	[177]	
CNT/UiO-66	AO7	80.6	π - π , Electrostatic	-	[177]	
GO/UiO-66	AO7	66.2	π - π , Electrostatic	-	[177]	
UiO-66	AY17	22.3	-	-	[177]	
CNT/UiO-66	AY17	86.4	π - π , Electrostatic	-	[177]	
GO/UiO-66	AY17	63.2	π - π , Electrostatic	-	[177]	

Kumar et al. [174] synthesized a cost-effective MOF-5/GO nanocomposite for RhB dye removal from the aquatic environment with a fast adsorption kinetic and an adsorption capacity of 151.62 mg/g at a 500 ppm concentration of dye solution.

Dadashi et al. [171] synthesized GO-copper-based MOF as an adsorbent for MB uptake from the aquatic environment with a high adsorption capacity of 173 mg/g compared to 106 mg/g for Cu-MOF at 25 °C. The π - π stacking would lead to the formation of a layered structure outperforming bare MOF. Moreover, the extra π - π interaction between GO and MB dye would enhance the adsorption capacity of the composite. Abdi et al. [172] synthesized ZIF, GO/ZIF, and CNT/ZIF to investigate the adsorptive separation of cationic MG dye from the aquatic environment. The maximum adsorption capacity of ZIF, GO/ZIF, and CNT/ZIF obtained was 1667, 3300, and 2667 mg/g at 293 K, respectively. The thermal stability of GO was low and its thermal decomposition occurred up to 200 °C. ZIF-8 presented excellent thermal stability up to 400 °C. The presence of ZIF-8 in the composite structure would improve the thermal stability of GO/ZIF-8 composites. In general, with elevation of the ZIF-8 content in composites, their thermal stability grew. As shown in Figure 7, the ZIF-8 ratio in composites directly affected the performance of the composites, where a higher adsorption capacity was obtained for composite with 70–90 wt.% ZIF-8 content. In this study, ZIF-8- and ZIF-8-based CNT and GO composites were introduced as excellent adsorbents with a highly efficient performance in dye removal from the aquatic environment. These superior materials outperformed other adsorbents in MG uptake, as reported in Table 12.

Table 12. Comparison of different adsorbents in MG removal from the aquatic environment; reprinted with permission from Ref. [172]. Copyright 2017 Elsevier.

Adsorbent	Removal (%)	Maximum Adsorption Capacity (mg/g)
Activated carbon	-	200
Nanoparticles on the ash	80	500
Chitosan bead		93.5
MIL-100(Fe)	88	485
MIL-53(Al)/NH ₂	76	164.9

ZIF-8	80	1667
GO/ZIF-8	92	3300
CNT/ZIF-8	97	2034

Zhao et al. [173] synthesized Ni-MOF and GO/Ni-MOF to investigate the removal of CR from water. The GO would create new pores at the interface of the composite, with the BET surface area being expanded from 59.8 for Ni-MOF to 69.6 for GO/Ni-MOF. The maximum adsorption capacity of the composite over CR adsorption obtained was 2489 and 2046 mg/g for GO/Ni-MOF and Ni-MOF, respectively. With functional groups such as –OH and –COOH provided by GO in the composite structure and strong electrostatic interactions between these functional groups and CR dye, the adsorption capacity of GO/Ni-MOF was higher than that of Ni-MOF.

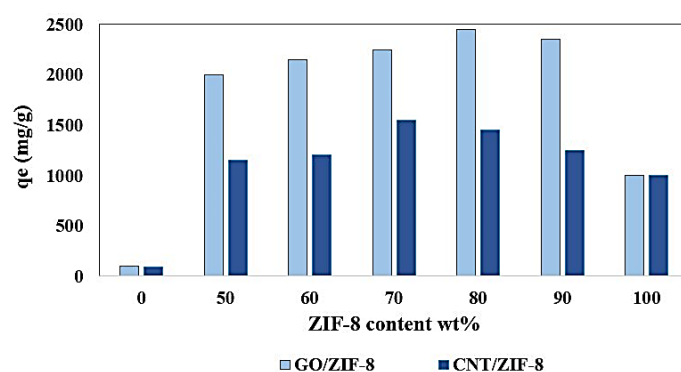


Figure 7. The effect of ZIF-8 contents on the adsorption capacity of GO/ZIF-8 and CNT/ZIF-8 composites. Reprinted with permission from Ref. [174]. Copyright 2018 Elsevier.

MIL-68(Al)/GO was prepared by Wu et al. [175] to examine the adsorption performance of the anionic MO dye from water. The maximum capacity for MO removal using MIL-68(Al) and MIL-68(Al)/GO was 340.14 and 400 mg/g, respectively. The rise in adsorption capacity was attributed to the enhanced BET surface area of the composite. Adding GO to the MIL-68(Al) structure would expand the BET surface area from 1239 to 1309 m²/g. H-bonding between oxygen or nitrogen atom of MO and –OH groups of Al–O–Al units in MIL-68(Al) structure was the main interaction in MO adsorption in this study. Adsorption properties of MIL-100(Fe) and GO/MIL-100(Fe) for an aqueous system containing MB and MO were compared by Luo et al. [176]. Their results revealed that the addition of 5% (*w/w*) GO in MOF contributed to a considerable growth in the adsorption capacity from 1019 mg/g to 1231 mg/g for MB and from 667 to 1189 mg/g for MO. Regarding the thermal stability, the decomposition temperature of the MOF rose from 280 to 350 °C with 5% GO. Further increase in the GO content reduced the adsorption capacity due to a decrement in the surface area and pore volume. At the GO content of 25% (*w/w*), GO sheets would cover the MOF structure and hinder dye adsorption on the active surface sites of MOF, resulting in a drop in the adsorption capacity.

Lin et al. [177] synthesized UiO-66, NH₂-UiO-66, GO/UiO-66, and CNT/UiO-66 to investigate the adsorption of two acid dyes including AO7 and AY17 from the aquatic environment. For AO7 adsorption, the maximum capacity obtained was 42.6, 55, 80.6, and 66.198 mg/g for UiO-66, NH₂-UiO-66, CNT/UiO-66, and GO/UiO-66, respectively. In the case of AY17 adsorption, the maximum capacity obtained was 22.3, 81.8, 86.4, and 63.2 mg/g for UiO-66, NH₂-UiO-66, CNT/UiO-66, and GO/UiO-66, respectively. CNT/UiO-66 indicated a better adsorption capacity toward both dyes. The electrostatic interactions between acidic sites on CNTs and nitrogen-containing functionalized groups would improve the adsorption performance. In addition to the best adsorption performance for CNT/UiO-66, this composite offered the best thermal stability compared to UiO-66, NH₂-UiO-66, and GO/UiO-66. The thermal decomposition of CNT/UiO-66 was around 510 °C,

while UiO-66 and GO/UiO-66 were decomposed within the range of 410–450 °C. The CNT by the surrounding UiO-66 structure would cause thermal decomposition at higher temperatures.

4. Effective Parameters on Dye Adsorption by MOFs

4.1. The Effect of pH on Dye Removal using MOFs

One of the most critical factors contributing to the removal of contaminants from the aquatic environment is pH [178]. The pH affects the surface charge and the adsorbent surface characteristics [179]. Concerning the type of dye and adsorbent, pH can have different effects on the adsorption performance of the adsorbent. The pH value at which the adsorbent surface area is neutral is known as the point of zero charge, an essential factor in identifying the nature of the active sites [180]. In the adsorption of cationic dyes by elevating the pH values from the point of zero charges, the electrostatic attraction between the adsorbate and the adsorbent increased and the adsorption capacity was enhanced. In the case of anionic dyes, it could enhance the adsorption capacity by reducing the pH value of the solution from the point of zero charge, creating a positive charge at the absorption area and promoting electrostatic attraction between the dye molecules and the adsorbent surface. Moreover, in the adsorption of cationic dyes in aqueous solutions with reduction in pH value and increase in H⁺ ions in the solution, competitive adsorption between dye molecules and H⁺ ions would lower the adsorption capacity. In anionic dyes, the same competitive adsorption between OH⁻ ions and dye molecules would lower the adsorption capacity [181,182]. The appropriate pH range for adsorption of some dyes by different MOFs is listed in Table 13.

Table 13. The optimum pH and p*H*_{pzc} values reported in the literature for dye removal using different MOF-based adsorbents.

MOFs	Dyes	p <i>H</i> _{pzc}	Ref.
Ni-BDC	MB	-	[183]
Fe ₃ O ₄ @AMCA-MIL-53(Al)	MB	5.6	[184]
Fe ₃ O ₄ @AMCA-MIL-53(Al)	MG	5.6	[184]
Fe ₃ O ₄ @MIL-100(Fe)	MR	-	[185]
Fe ₃ O ₄ @MIL-100(Fe)	MB		[186]
PCN-222	MB	8	[86]
PCN-222	MO	8	[86]
Cu-BTC	MB	4	[89]
MIL-68(In)	CR	-	[77]
UiO-67	CR	5.7	[85]
TMU-8	RB5	-	[93]
MIL-53(Fe)	MR	-	[80]
UiO-66	MB	-	[68]
UiO-66	MO	-	[68]
UiO-66	MB	6	[82]
MIL-68(Al)	MO	-	[75]
MIL-53(Al)	MG	4.4	[97]
MIL-53(Al)	MO	4.4	[97]
MIL-125(Ti)	RhB	-	[76]
MIL-100(Fe)	CR	-	[78]

Alqadami et al. [184], in adsorptive removal of MB and MG dyes by Fe₃O₄@AMCA-MIL-53(Al), observed that by increasing pH from 2 to 6.8 for MG, the adsorption capacity rose from 10.5 to 28.5 mg/g, and for MB by elevating pH from 1.5 to 8.9, q_e (i.e., the adsorption capacity at equilibrium) increased from 10.2 to 27.7 mg/g. At pHs above 5.6, the

adsorbent surface would take on a negative charge and efficiently uptake cationic MB plus MG dyes. Dadfarnia et al. [185] synthesized $\text{Fe}_3\text{O}_4@\text{MIL-100}(\text{Fe})$ and examined its ability to remove MR. They concluded that by increasing the pH from 2 to 10, the adsorption capacity diminished from 555 mg/g to 310 mg/g. This indicates the placement of methyl red between anionic dyes. By elevating the pH value, the positively charged sites of the adsorbent would diminish, and so would the amount of adsorbed MR. In another study by Shao et al. [186] on the adsorption of MB by $\text{Fe}_3\text{O}_4@\text{MIL-100}(\text{Fe})$, it was concluded that upon enhancing the pH value from 2 to 9, q_e rose from 28 mg/g to 42 mg/g. The increase in pH would augment the negative charge on the MOF surface, causing higher electrostatic attraction and π - π stacking between MB and the MOF surface.

In some cases, the effect of pH on the structure of MOF also had a significant effect on the adsorption performance, where low or high pHs could damage the MOFs structure. Al Sharbati et al. [97] in MO and MG adsorption found that the decline in MIL-53 adsorption capacity at pHs above 8 was due to the structural degradation at alkaline pHs. In general, in examining the effect of pH on adsorption experiments, the stability of the structure in acidic and alkaline environments should also be considered. Some MOFs such as UiO-66 [187], MIL-101(Cr) [187], PCN-225 [188], PCN-228 [189], and PCN-600(Fe) [190] have considerable stability in acidic and alkaline environments.

4.2. The Effect of Adsorbent Dosage on Dye Removal Using MOFs

Another important parameter in adsorption is the initial dosage of the adsorbent, which determines the cost of adsorption and removal of pollutants. As the amount of adsorbent increased, due to the increased number of available active sites, so did the adsorption rate. An optimal value of adsorbent amount can help improve the adsorption process. This is because less adsorbent content can reduce the adsorption capacity, while the extra amount will result in additional costs. In general, with elevating the initial adsorbent dosage, the adsorption capacity would diminish, while the removal efficiency grows. In a study examining the effect of adsorbent dose on MG and MB removal via $\text{Fe}_3\text{O}_4@\text{MIL-53}(\text{Al})$ by Alqadami et al. [184], it was found that by elevating the adsorbent dosage up to 100 mg, the adsorption capacity of both dyes dropped from 27.9 to 5.8 mg/g and from 28.2 to 5.9 mg/g. The aggregation of adsorbent particles and reduction in the surface area would lead to a decrement in the adsorption capacity. In contrast, with the augmentation of adsorbent dosage, the removal efficiency of MG and MB increased by 89.4–93.8% and 90–94.6%, respectively, due to the increase in active adsorption sites. In the study of MB removal using UiO-66 by Mohammadi et al. [82], the removal efficiency rose from 30 to 70% by increasing the initial UiO-66 dosage from 0.1 to 0.5 g/L. In another study by Yaoyao et al. [98], the percentage of adsorption of methyl blue and MB increased by 65–80% and 75–99%, respectively, by heightening the initial MIL-100(Fe) dosage from 1 to 50 mg.

In general, MOFs, with their large surface area and ultra-porous structures, require lower doses than other adsorbents for wastewater treatment applications. The high surface area of the MOFs could allow them to provide larger number of active sites for the adsorption of contaminant molecules and a high adsorption capacity.

4.3. The Effect of Contact Time on Dye Removal Using MOFs

The adsorption capacity would grow with increased contact time, though there must be an optimal contact time during the uptake. Active adsorption sites are gradually covered with the adsorbent during the adsorption process, and after a specific time, the adsorbent cannot absorb more dye molecules, which is called equilibrium time [191]. Over time, active sites of adsorbent are occupied by dye molecules and the adsorbent can no longer adsorb more dyes, whereby the adsorption process stops [192,193]. Most MOFs need a very short time to reach the equilibrium point of adsorption [86,89,92,93,95,184]. Fast adsorption may be due to various interactions between MOF and contaminant molecules. Duo et al. [91] confirmed the fast adsorption of CR and LY over MOF-235 due to

the hydrophobic nature of MOF and dye molecules. In these experiments, both dyes were adsorbed onto MOF-235 within less than 15 min. In some cases, the formation of bonds between MOF groups and dye molecules caused fast adsorption. In the study of removal of methyl blue by ZIF-8 by Feng et al. [87], the effect of ZnO bonding with dye molecules on fast adsorption was confirmed. The adsorption equilibrium was reached within less than 30 min in this experiment.

4.4. The Effect of Initial Dye Concentration on Dye Removal Using MOFs

At low initial concentrations, the removal efficiency is intense, and the adsorption process is rapidly equilibrated. The adsorption rate would diminish as the initial concentration grows due to the saturation of active sites of the MOF [194,195]. In general, at a constant adsorbent dose, the amount of adsorption grows with elevation of the initial dye concentration, which may be related to the rise in the concentration gradient. In contrast, with increasing initial dye concentration due to saturation of adsorption sites, the removal percentage would decline [97,172].

5. Conclusions

Metal–organic frameworks with superior advantages over other conventional sorbents in removing dyes from the aquatic environment have attracted much attention in recent years. Extensive structural diversity, the possibility of using different structures with different metal clusters and/or organic linkers according to the purpose, is one of the most important characteristics of MOFs in the field of wastewater treatment, which distinguishes them from other adsorbents. MIL-type MOF structures with adjustable properties for selective adsorption, ZIF structures with high surface area and high adsorption capacity, and zirconium-based MOFs with excellent stability in aqueous and acidic environments are categorized as the most studied structures in dye removal applications. The removal of various dyes such as methylene blue, methyl orange, Congo red, acid orange 7, malachite green, acid chrome blue K, acid red 1, orange G, methyl red, basic blue 41, rhodamine B, neutral red, fuchsin basic, safranin T, alizarin red S, eosin, fuchsin acid, reactive black 5, xylene orange, fluorescein sodium, and sunset yellow have been studied using MOF-based sorbents. The existence of some challenges such as stability in aqueous and acidic environments, reusability, and improvement of adsorption performance through increasing the adsorption capacity has led researchers to modify and structurally improve metal–organic frameworks. Synthesis of magnetic MOF-based composites for easy recycling and reuse, introduction of amine functional groups, and preparation of graphene–MOF composites to increase the adsorption capacity and improve the stability of the framework in the aqueous medium are some of the proposed and applied solutions to address the above-mentioned challenges. Amine-functionalized MOF structures aim to increase the adsorption capacity by creating and improving hydrogen bonds and electrostatic interactions between the dye molecules and the adsorbent framework. Use of graphene–MOF composites also aims to increase the adsorption capacity by improving electrostatic and π – π interactions. These composites also have high thermal stability due to their sandwich-shaped structures and the presence of graphene in the structure.

Author Contributions: Conceptualization, F.H.S. and M.A.; methodology, F.H.S., A.B. and M.A.; formal analysis, M.B., F.H.S., V.V.K. and M.A.; investigation, M.B., V.V.K. and F.H.S.; resources, F.H.S., A.B. and M.A.; writing—original draft preparation, M.B. and V.V.K.; writing—review and editing, F.H.S., A.B. and M.A.; visualization, M.B., supervision, F.H.S. and M.A. All authors have read and agreed to the published version of the manuscript.

Funding: M.A. was supported by Swiss National Science Foundation, under grant number P2ELP2_195134.

Institutional Review Board Statement: Not applicable.

Informed Consent Statement: Not applicable.

Data Availability Statement: Not applicable.

Acknowledgments: M.A. acknowledges a fellowship from the Swiss National Science Foundation (P2ELP2_195134).

Conflicts of Interest: The authors declare no conflict of interest.

Abbreviations

HKUST-1	Cu ₃ (BTC) ₂
TMU-39	[Zn ₄ (oba) ₃ (DMF) ₂]
TMU-7	[Cd(oba)(4-bdph)] _n .DMF
ZIF	Zeolitic imidazolate framework
TMU-16	[Zn ₂ (BDC) ₂ (4-bpdh)].3DMF
ZIF	Zeolitic Imidazolate Frameworks
NU	Northwestern University
UiO	Universitetet i Oslo
MIL	Material Institute Lavoisier
PCN	Porous coordination network
GO	Graphene oxide
CNT	Carbon nanotube
L	1,4-bis(4-pyridyl)-2,3-diaza-1,3-butadiene
4,4'-BPpy	4,4'-Bipyridine
BDC	Benzene-1,4-dicarboxylic acid
H2oba	4,4'-oxy(bis)benzoic acid
bpe	1,2-bis(4-pyridyl)ethene
DMA	N,N'-dimethylacetamide
BTC	benzene-1,3,5-tricarboxylate
H3lmdc	4,5-imidazole dicarboxylic acid
BPDC	biphenyldicarboxylic acid
BPB	1,4-bis(4'-pyrazolyl)benzene
MB	Methylene blue
MO	Methyl orange
CR	Congo red
AO7	Acid orange 7
AB1	Acid black 1
MG	Malachite green
SY	Sunset yellow
LY	Lemon yellow
AC	Acid chrome blue K
AR1	Acid red 1
OG	Orange G
RB-B	Rose-bengal B
ARS	Alizarin red S
FA	Fuchsin acid
XO	Xylenol orange
FS	Fluorescein sodium
MR	Methyl red
IC	Indigo carmine
BR46	Basic red 46
BB41	Basic blue 41
RhB	Rhodamine B
PPCP	Pharmaceutical and personal care product
MMT-CTAB	Cetyltrimethylammonium bromide modified clays

References

1. Yang, C.; Xu, W.; Nan, Y.; Wang, Y.; Chen, X. Novel negatively charged nanofiltration membrane based on 4,4'-diaminodiphenylmethane for dye removal. *Sep. Purif. Technol.* **2020**, *248*, 117089. <https://doi.org/10.1016/j.seppur.2020.117089>.

2. Yang, X.; Wang, D. Photocatalysis: From Fundamental Principles to Materials and Applications. *ACS Appl. Energy Mater.* **2018**, *1*, 6657–6693. <https://doi.org/10.1021/acsaem.8b01345>.
3. Maleki, H.; Hüsing, N. Current status, opportunities and challenges in catalytic and photocatalytic applications of aerogels: Environmental protection aspects. *Appl. Catal. B Environ.* **2018**, *221*, 530–555. <https://doi.org/10.1016/j.apcatb.2017.08.012>.
4. Hooriabad Saboor, F.; Nasirpour, N.; Shahsavari, S.; Kazemian, H. The Effectiveness of MOFs for the Removal of Pharmaceuticals from Aquatic Environments: A Review Focused on Antibiotics Removal. *Chem. Asian J.* **2022**, *17*, e202101105. <https://doi.org/10.1002/asia.202101105>.
5. Hu, N.; Zhang, K.; Zhao, Y.; Zhang, Z.; Li, H. Flotation-based dye removal system: Sweet potato protein fabricated from agro-industrial waste as a collector and frother. *J. Clean. Prod.* **2020**, *269*, 122121, <https://doi.org/10.1016/j.jclepro.2020.122121>.
6. Phan, D.-N.; Rebia, R.A.; Saito, Y.; Kharaghani, D.; Khatri, M.; Tanaka, T.; Lee, H.; Kim, I.-S. Zinc oxide nanoparticles attached to polyacrylonitrile nanofibers with hinokitiol as gluing agent for synergistic antibacterial activities and effective dye removal. *J. Ind. Eng. Chem.* **2020**, *85*, 258–268. <https://doi.org/10.1016/j.jiec.2020.02.008>.
7. Ravikumar, K.; Deebika, B.; Balu, K. Decolourization of aqueous dye solutions by a novel adsorbent: Application of statistical designs and surface plots for the optimization and regression analysis. *J. Hazard. Mater.* **2005**, *122*, 75–83. <https://doi.org/10.1016/j.jhazmat.2005.03.008>.
8. Bensalah, N.; Alfaro, M.A.Q.; Martínez-Huitle, C.A. Electrochemical treatment of synthetic wastewaters containing Alphazurine A dye. *Chem. Eng. J.* **2009**, *149*, 348–352. <https://doi.org/10.1016/j.cej.2008.11.031>.
9. Dawood, S.; Sen, T.K.; Phan, C. Synthesis and Characterisation of Novel-Activated Carbon from Waste Biomass Pine Cone and Its Application in the Removal of Congo Red Dye from Aqueous Solution by Adsorption. *Water Air Soil Pollut.* **2013**, *225*, 1818. <https://doi.org/10.1007/s11270-013-1818-4>.
10. Jadhav, S.A.; Garud, H.B.; Patil, A.H.; Patil, G.D.; Patil, C.R.; Dongale, T.D.; Patil, P.S. Recent advancements in silica nanoparticles based technologies for removal of dyes from water. *Colloid Interface Sci. Commun.* **2019**, *30*, 100181. <https://doi.org/10.1016/j.colcom.2019.100181>.
11. Gupta, V.K.; Suhas. Application of low-cost adsorbents for dye removal—A review. *J. Environ. Manag.* **2009**, *90*, 2313–2342. <https://doi.org/10.1016/j.jenvman.2008.11.017>.
12. Gupta, V.K.; Kumar, R.; Nayak, A.; Saleh, T.A.; Barakat, M.A. Adsorptive removal of dyes from aqueous solution onto carbon nanotubes: A review. *Adv. Colloid Interface Sci.* **2013**, *193–194*, 24–34. <https://doi.org/10.1016/j.cis.2013.03.003>.
13. Clarke, E.A.; Anliker, R. Organic Dyes and Pigments. In *Anthropogenic Compounds*; Anliker, R., Butler, G.C., Clarke, E.A., Förstner, U., Funke, W., Hyslop, C., Kaiser, G., Rappe, C., Russow, J., Tölg, G., et al., Eds.; Springer: Berlin/Heidelberg, Germany, 1980; pp. 181–215. https://doi.org/10.1007/978-3-540-38522-6_7.
14. Al-Ghouti, M.A.; Sweleh, A.O. Optimizing textile dye removal by activated carbon prepared from olive stones. *Environ. Technol. Innov.* **2019**, *16*, 100488. <https://doi.org/10.1016/j.eti.2019.100488>.
15. Biswas, S.; Mohapatra, S.S.; Kumari, U.; Meikap, B.C.; Sen, T.K. Batch and continuous closed circuit semi-fluidized bed operation: Removal of MB dye using sugarcane bagasse biochar and alginate composite adsorbents. *J. Environ. Chem. Eng.* **2020**, *8*, 103637. <https://doi.org/10.1016/j.jece.2019.103637>.
16. Khajeh, M.; Amin, M.M.; Taheri, E.; Fatehizadeh, A.; McKay, G. Influence of co-existing cations and anions on removal of direct red 89 dye from synthetic wastewater by hydrodynamic cavitation process: An empirical modeling. *Ultrason. Sonochem.* **2020**, *67*, 105133. <https://doi.org/10.1016/j.ultsonch.2020.105133>.
17. Kandisa, R.; Saibaba, K.V.N.; Shaik, K.B.; Gopinath, R. Dye Removal by Adsorption: A Review. *J. Bioremediat. Biodegrad.* **2016**, *7*, 371. <https://doi.org/10.4172/2155-6199.1000371>.
18. Shi, B.; Li, G.; Wang, D.; Feng, C.; Tang, H. Removal of direct dyes by coagulation: The performance of preformed polymeric aluminum species. *J. Hazard. Mater.* **2007**, *143*, 567–574. <https://doi.org/10.1016/j.jhazmat.2006.09.076>.
19. Zhao, P.; Wang, J.; Han, X.; Liu, J.; Zhang, Y.; Van der Bruggen, B. Zr-Porphyrin Metal–Organic Framework-Based Photocatalytic Self-Cleaning Membranes for Efficient Dye Removal. *Ind. Eng. Chem. Res.* **2021**, *60*, 1850–1858. <https://doi.org/10.1021/acs.iecr.0c05583>.
20. Yagub, M.T.; Sen, T.K.; Afroze, S.; Ang, H.M. Dye and its removal from aqueous solution by adsorption: A review. *Adv. Colloid Interface Sci.* **2014**, *209*, 172–184. <https://doi.org/10.1016/j.cis.2014.04.002>.
21. Nidheesh, P.V.; Zhou, M.; Oturan, M.A. An overview on the removal of synthetic dyes from water by electrochemical advanced oxidation processes. *Chemosphere* **2018**, *197*, 210–227. <https://doi.org/10.1016/j.chemosphere.2017.12.195>.
22. Pandit, P.; Basu, S. Dye and Solvent Recovery in Solvent Extraction Using Reverse Micelles for the Removal of Ionic Dyes. *Ind. Eng. Chem. Res.* **2004**, *43*, 7861–7864. <https://doi.org/10.1021/ie0402160>.
23. Palanisamy, S.; Nachimuthu, P.; Awasthi, M.K.; Ravindran, B.; Chang, S.W.; Palanichamy, M.; Nguyen, D.D. Application of electrochemical treatment for the removal of triazine dye using aluminium electrodes. *J. Water Supply Res. Technol.-Aqua* **2020**, *69*, 345–354. <https://doi.org/10.2166/aqua.2020.109>.
24. Bhatia, D.; Sharma, N.; Singh, J.; Kanwar, R. Biological methods for textile dye removal from wastewater: A Review. *Crit. Rev. Environ. Sci. Technol.* **2017**, *47*, 1836–1876. <https://doi.org/10.1080/10643389.2017.1393263>.
25. Fang, W.H.; Zhang, L.; Zhang, J.; Yang, G.Y. Water-Stable Homochiral Cluster Organic Frameworks Built by Two Kinds of Large Tetrahedral Cluster Units. *Chemistry* **2016**, *22*, 2611–2615. <https://doi.org/10.1002/chem.201505125>.
26. Nandasiri, M.I.; Jambovane, S.R.; McGrail, B.P.; Schaef, H.T.; Nune, S.K. Adsorption, separation, and catalytic properties of densified metal-organic frameworks. *Coord. Chem. Rev.* **2016**, *311*, 38–52. <https://doi.org/10.1016/j.ccr.2015.12.004>.

27. Kadhom, M.; Albayati, N.; Alalwan, H.; Al-Furaiji, M. Removal of dyes by agricultural waste. *Sustain. Chem. Pharm.* **2020**, *16*, 100259. <https://doi.org/10.1016/j.scp.2020.100259>.
28. Pathania, D.; Sharma, S.; Singh, P. Removal of methylene blue by adsorption onto activated carbon developed from *Ficus carica* bast. *Arab. J. Chem.* **2017**, *10*, S1445–S1451. <https://doi.org/10.1016/j.arabjc.2013.04.021>.
29. De Gisi, S.; Lofrano, G.; Grassi, M.; Notarnicola, M. Characteristics and adsorption capacities of low-cost sorbents for wastewater treatment: A review. *Sustain. Mater. Technol.* **2016**, *9*, 10–40. <https://doi.org/10.1016/j.susmat.2016.06.002>.
30. Kyzas, G.Z.; Kostoglou, M. Green Adsorbents for Wastewaters: A Critical Review. *Materials* **2014**, *7*, 333–364. <https://doi.org/10.3390/ma7010333>.
31. Abbasi, Z.; Cseri, L.; Zhang, X.; Ladewig, B.P.; Wang, H. Chapter 7—Metal–Organic Frameworks (MOFs) and MOF-Derived Porous Carbon Materials for Sustainable Adsorptive Wastewater Treatment. In *Sustainable Nanoscale Engineering*; Szekely, G., Livingston, A., Eds.; Elsevier: Amsterdam, The Netherlands, 2020; pp. 163–194. <https://doi.org/10.1016/B978-0-12-814681-1.00007-2>.
32. Wen, M.; Li, G.; Liu, H.; Chen, J.; An, T.; Yamashita, H. Metal–organic framework-based nanomaterials for adsorption and photocatalytic degradation of gaseous pollutants: Recent progress and challenges. *Environ. Sci. Nano* **2019**, *6*, 1006–1025. <https://doi.org/10.1039/C8EN01167B>.
33. Li, H.-Y.; Zhao, S.-N.; Zang, S.-Q.; Li, J. Functional metal–organic frameworks as effective sensors of gases and volatile compounds. *Chem. Soc. Rev.* **2020**, *49*, 6364–6401. <https://doi.org/10.1039/C9CS00778D>.
34. Mason, J.A.; Veenstra, M.; Long, J.R. Evaluating metal–organic frameworks for natural gas storage. *Chem. Sci.* **2014**, *5*, 32–51. <https://doi.org/10.1039/C3SC52633J>.
35. Qiu, T.; Liang, Z.; Guo, W.; Tabassum, H.; Gao, S.; Zou, R. Metal–Organic Framework-Based Materials for Energy Conversion and Storage. *ACS Energy Lett.* **2020**, *5*, 520–532. <https://doi.org/10.1021/acscenergylett.9b02625>.
36. Orellana-Tavra, C.; Marshall, R.J.; Baxter, E.F.; Lázaro, I.A.; Tao, A.; Cheetham, A.K.; Forgan, R.S.; Fairen-Jimenez, D. Drug delivery and controlled release from biocompatible metal–organic frameworks using mechanical amorphization. *J. Mater. Chem. B* **2016**, *4*, 7697–7707. <https://doi.org/10.1039/C6TB02025A>.
37. Valizadeh, B.; Nguyen, T.N.; Stylianou, K.C. Shape engineering of metal–organic frameworks. *Polyhedron* **2018**, *145*, 1–15. <https://doi.org/10.1016/j.poly.2018.01.004>.
38. Beydaghdari, M.; Saboor, F.H.; Babapoor, A.; Asgari, M. Recent Progress in Adsorptive Removal of Water Pollutants by Metal–Organic Frameworks. *ChemNanoMat* **2022**, *8*, e202100400. <https://doi.org/10.1002/cnma.202100400>.
39. Au, V.K.-M. Recent Advances in the Use of Metal–Organic Frameworks for Dye Adsorption. *Front. Chem.* **2020**, *8*, 708. <https://doi.org/10.3389/fchem.2020.00708>.
40. Denisov, G.L.; Primakov, P.V.; Korlyukov, A.A.; Novikov, V.V.; Nelyubina, Y.V. Solvothermal Synthesis of the Metal–Organic Framework MOF-5 in Autoclaves Prepared by 3D Printing. *Russ. J. Coord. Chem.* **2019**, *45*, 836–842. <https://doi.org/10.1134/S1070328419120030>.
41. Hu, Z.; Kundu, T.; Wang, Y.; Sun, Y.; Zeng, K.; Zhao, D. Modulated Hydrothermal Synthesis of Highly Stable MOF-808(Hf) for Methane Storage. *ACS Sustain. Chem. Eng.* **2020**, *8*, 17042–17053. <https://doi.org/10.1021/acssuschemeng.0c04486>.
42. Beamish-Cook, J.; Shankland, K.; Murray, C.A.; Vaqueiro, P. Insights into the Mechanochemical Synthesis of MOF-74. *Cryst. Growth Des.* **2021**, *21*, 3047–3055. <https://doi.org/10.1021/acs.cgd.1c00213>.
43. Son, W.-J.; Kim, J.; Kim, J.; Ahn, W.-S. Sonochemical synthesis of MOF-5. *Chem. Commun.* **2008**, *44*, 6336–6338. <https://doi.org/10.1039/B814740J>.
44. Troyano, J.; Çamur, C.; Garzón-Tovar, L.; Carné-Sánchez, A.; Imaz, I.; MasPOCH, D. Spray-Drying Synthesis of MOFs, COFs, and Related Composites. *Acc. Chem. Res.* **2020**, *53*, 1206–1217. <https://doi.org/10.1021/acs.accounts.0c00133>.
45. Sumida, K.; Liang, K.; Reboul, J.; Ibarra, I.A.; Furukawa, S.; Falcaro, P. Sol–Gel Processing of Metal–Organic Frameworks. *Chem. Mater.* **2017**, *29*, 2626–2645. <https://doi.org/10.1021/acs.chemmater.6b03934>.
46. Bayliss, P.A.; Ibarra, I.A.; Pérez, E.; Yang, S.; Tang, C.C.; Poliakov, M.; Schröder, M. Synthesis of metal–organic frameworks by continuous flow. *Green Chem.* **2014**, *16*, 3796–3802. <https://doi.org/10.1039/C4GC00313F>.
47. Ghanbari, T.; Abnisa, F.; Wan Daud, W.M.A. A review on production of metal organic frameworks (MOF) for CO₂ adsorption. *Sci. Total Environ.* **2020**, *707*, 135090. <https://doi.org/10.1016/j.scitotenv.2019.135090>.
48. Martin, R.L.; Haranczyk, M. Exploring frontiers of high surface area metal–organic frameworks. *Chem. Sci.* **2013**, *4*, 1781–1785. <https://doi.org/10.1039/C3SC00033H>.
49. Howarth, A.; Liu, Y.; Li, Z.; Wang, T.; Hupp, J.; Farha, O. Chemical, thermal and mechanical stabilities of metal–organic frameworks. *Nat. Rev. Mater.* **2016**, *1*, 15018. <https://doi.org/10.1038/natrevmats.2015.18>.
50. Ibrahim, A.O.; Adegoke, K.A.; Adegoke, R.O.; AbdulWahab, Y.A.; Oyelami, V.B.; Adesina, M.O. Adsorptive removal of different pollutants using metal–organic framework adsorbents. *J. Mol. Liq.* **2021**, *333*, 115593. <https://doi.org/10.1016/j.molliq.2021.115593>.
51. Farha, O.; Eryazici, I.; Jeong, N.C.; Hauser, B.; Wilmer, C.; Sarjeant, A.; Snurr, R.; Nguyen, S.; Yazaydin, A.; Hupp, J. Metal–Organic Framework Materials with Ultrahigh Surface Areas: Is the Sky the Limit? *J. Am. Chem. Soc.* **2012**, *134*, 15016–15021. <https://doi.org/10.1021/ja3055639>.
52. Haldar, D.; Duarah, P.; Purkait, M.K. MOFs for the treatment of arsenic, fluoride and iron contaminated drinking water: A review. *Chemosphere* **2020**, *251*, 126388. <https://doi.org/10.1016/j.chemosphere.2020.126388>.

53. Gautam, S.; Agrawal, H.; Thakur, M.; Akbari, A.; Sharda, H.; Kaur, R.; Amini, M. Metal oxides and metal organic frameworks for the photocatalytic degradation: A review. *J. Environ. Chem. Eng.* **2020**, *8*, 103726. <https://doi.org/10.1016/j.jece.2020.103726>.
54. Jiang, D.; Chen, M.; Wang, H.; Zeng, G.; Huang, D.; Cheng, M.; Liu, Y.; Xue, W.; Wang, Z. The application of different typological and structural MOFs-based materials for the dyes adsorption. *Coord. Chem. Rev.* **2019**, *380*, 471–483. <https://doi.org/10.1016/j.ccr.2018.11.002>.
55. Furukawa, H.; Cordova, K.E.; O’Keeffe, M.; Yaghi, O.M. The chemistry and applications of metal-organic frameworks. *Science* **2013**, *341*, 1230444. <https://doi.org/10.1126/science.1230444>.
56. Makal, T.A.; Wang, X.; Zhou, H.-C. Tuning the Moisture and Thermal Stability of Metal–Organic Frameworks through Incorporation of Pendant Hydrophobic Groups. *Cryst. Growth Des.* **2013**, *13*, 4760–4768. <https://doi.org/10.1021/cg4009224>.
57. Tan, K.; Nijem, N.; Gao, Y.; Zuluaga, S.; Li, J.; Thonhauser, T.; Chabal, Y.J. Water interactions in metal organic frameworks. *CrystEngComm* **2015**, *17*, 247–260. <https://doi.org/10.1039/C4CE01406E>.
58. Čelič, T.B.; Mazaj, M.; Mali, G.; Kaučič, V.; Logar, N.Z. Hydrothermal Stability As an Important Characteristics of Metal-Organic Framework Materials. In Proceedings of the 5th Serbian-Croatian-Slovenian Symposium on Zeolites, Čajetina, Serbia, 30 May–2 June 2013.
59. Dhaka, S.; Kumar, R.; Deep, A.; Kurade, M.B.; Ji, S.-W.; Jeon, B.-H. Metal–organic frameworks (MOFs) for the removal of emerging contaminants from aquatic environments. *Coord. Chem. Rev.* **2019**, *380*, 330–352. <https://doi.org/10.1016/j.ccr.2018.10.003>.
60. Yaghi, O.M.; O’Keeffe, M.; Ockwig, N.W.; Chae, H.K.; Eddaoudi, M.; Kim, J. Reticular synthesis and the design of new materials. *Nature* **2003**, *423*, 705–714. <https://doi.org/10.1038/nature01650>.
61. Ferey, G.; Mellot-Draznieks, C.; Serre, C.; Millange, F.; Dutour, J.; Surble, S.; Margiolaki, I. A chromium terephthalate-based solid with unusually large pore volumes and surface area. *Science* **2005**, *309*, 2040–2042. <https://doi.org/10.1126/science.1116275>.
62. Kirchon, A.; Feng, L.; Drake, H.F.; Joseph, E.A.; Zhou, H.-C. From fundamentals to applications: A toolbox for robust and multifunctional MOF materials. *Chem. Soc. Rev.* **2018**, *47*, 8611–8638. <https://doi.org/10.1039/C8CS00688A>.
63. Drout, R.J.; Robison, L.; Chen, Z.; Islamoglu, T.; Farha, O.K. Zirconium Metal–Organic Frameworks for Organic Pollutant Adsorption. *Trends Chem.* **2019**, *1*, 304–317. <https://doi.org/10.1016/j.trechm.2019.03.010>.
64. Ahmad, K.; Shah, H.-U.-R.; Parveen, S.; Aziz, T.; Naseem, H.A.; Ashfaq, M.; Rauf, A. Metal Organic Framework (KIUB-MOF-1) as efficient adsorbent for cationic and anionic dyes from brackish water. *J. Mol. Struct.* **2021**, *1242*, 130898. <https://doi.org/10.1016/j.molstruc.2021.130898>.
65. Tran Ba, L. Dye Adsorption on UiO-66: The Importance of Electrostatic Attraction Mechanism. *J. Water Chem. Technol.* **2020**, *42*, 441–449. <https://doi.org/10.3103/S1063455X20060107>.
66. Yu, C.-X.; Chen, J.; Zhang, Y.; Song, W.-B.; Li, X.-Q.; Chen, F.-J.; Zhang, Y.-J.; Liu, D.; Liu, L.-L. Highly efficient and selective removal of anionic dyes from aqueous solution by using a protonated metal-organic framework. *J. Alloys Compd.* **2021**, *853*, 157383. <https://doi.org/10.1016/j.jallcom.2020.157383>.
67. Tian, S.; Xu, S.; Liu, J.; He, C.; Xiong, Y.; Feng, P. Highly efficient removal of both cationic and anionic dyes from wastewater with a water-stable and eco-friendly Fe-MOF via host-guest encapsulation. *J. Clean. Prod.* **2019**, *239*, 117767. <https://doi.org/10.1016/j.jclepro.2019.117767>.
68. Yang, J.-M.; Ying, R.-J.; Han, C.-X.; Hu, Q.-T.; Xu, H.-M.; Li, J.-H.; Wang, Q.; Zhang, W. Adsorptive removal of organic dyes from aqueous solution by a Zr-based metal–organic framework: Effects of Ce(III) doping. *Dalton Trans.* **2018**, *47*, 3913–3920. <https://doi.org/10.1039/C8DT00217G>.
69. Firoozi, M.; Rafiee, Z.; Dashtian, K. New MOF/COF Hybrid as a Robust Adsorbent for Simultaneous Removal of Auramine O and Rhodamine B Dyes. *ACS Omega* **2020**, *5*, 9420–9428. <https://doi.org/10.1021/acsomega.0c00539>.
70. Hasan, Z.; Tong, M.; Jung, B.K.; Ahmed, I.; Zhong, C.; Jhung, S.H. Adsorption of Pyridine over Amino-Functionalized Metal–Organic Frameworks: Attraction via Hydrogen Bonding versus Base–Base Repulsion. *J. Phys. Chem. C* **2014**, *118*, 21049–21056. <https://doi.org/10.1021/jp507074x>.
71. Razavi, S.A.A.; Masoomi, M.Y.; Morsali, A. Host–Guest Interaction Optimization through Cavity Functionalization for Ultra-Fast and Efficient Water Purification by a Metal–Organic Framework. *Inorg. Chem.* **2018**, *57*, 11578–11587. <https://doi.org/10.1021/acs.inorgchem.8b01611>.
72. Leng, F.; Wang, W.; Zhao, X.J.; Hu, X.L.; Li, Y.F. Adsorption interaction between a metal–organic framework of chromium–benzenedicarboxylates and uranine in aqueous solution. *Colloids Surf. A Physicochem. Eng. Asp.* **2014**, *441*, 164–169. <https://doi.org/10.1016/j.colsurfa.2013.08.074>.
73. Tong, M.; Liu, D.; Yang, Q.; Devautour-Vinot, S.; Maurin, G.; Zhong, C. Influence of framework metal ions on the dye capture behavior of MIL-100 (Fe, Cr) MOF type solids. *J. Mater. Chem. A* **2013**, *1*, 8534–8537. <https://doi.org/10.1039/C3TA11807J>.
74. Tehrani, M.S.; Zare-Dorabei, R. Competitive removal of hazardous dyes from aqueous solution by MIL-68(Al): Derivative spectrophotometric method and response surface methodology approach. *Spectrochim. Acta Part A Mol. Biomol. Spectrosc.* **2016**, *160*, 8–18. <https://doi.org/10.1016/j.saa.2016.02.002>.
75. Wu, S.C.; You, X.; Yang, C.; Cheng, J.H. Adsorption behavior of methyl orange onto an aluminum-based metal organic framework, MIL-68(Al). *Water Sci. Technol.* **2017**, *75*, 2800–2810. <https://doi.org/10.2166/wst.2017.154>.
76. Guo, H.; Lin, F.; Chen, J.; Li, F.; Weng, W. Metal–organic framework MIL-125(Ti) for efficient adsorptive removal of Rhodamine B from aqueous solution. *Appl. Organometal. Chem.* **2015**, *29*, 12–19. <https://doi.org/10.1002/aoc.3237>.
77. Jin, L.-N.; Qian, X.-Y.; Wang, J.-G.; Aslan, H.; Dong, M. MIL-68 (In) nano-rods for the removal of Congo red dye from aqueous solution. *J. Colloid Interface Sci.* **2015**, *453*, 270–275. <https://doi.org/10.1016/j.jcis.2015.05.005>.

78. Moradi, S.E.; Dadfarnia, S.; Haji Shabani, A.M.; Emami, S. Removal of congo red from aqueous solution by its sorption onto the metal organic framework MIL-100(Fe): Equilibrium, kinetic and thermodynamic studies. *Desalin. Water Treat.* **2015**, *56*, 709–721. <https://doi.org/10.1080/19443994.2014.947328>.
79. Tsai, F.-C.; Xia, Y.; Ma, N.; Shi, J.-J.; Jiang, T.; Chiang, T.-C.; Zhang, Z.-C.; Tsen, W.-C. Adsorptive removal of acid orange 7 from aqueous solution with metal–organic framework material, iron (III) trimesate. *Desalin. Water Treat.* **2016**, *57*, 3218–3226. <https://doi.org/10.1080/19443994.2014.982199>.
80. Yilmaz, E.; Sert, E.; Atalay, F.S. Synthesis, characterization of a metal organic framework: MIL-53 (Fe) and adsorption mechanisms of methyl red onto MIL-53 (Fe). *J. Taiwan Inst. Chem. Eng.* **2016**, *65*, 323–330. <https://doi.org/10.1016/j.jtice.2016.05.028>.
81. Embaby, M.S.; Elwany, S.D.; Setyaningsih, W.; Saber, M.R. The adsorptive properties of UiO-66 towards organic dyes: A record adsorption capacity for the anionic dye Alizarin Red S. *Chin. J. Chem. Eng.* **2018**, *26*, 731–739. <https://doi.org/10.1016/j.cjche.2017.07.014>.
82. Mohammadi, A.A.; Alinejad, A.; Kamarehie, B.; Javan, S.; Ghaderpoury, A.; Ahmadpour, M.; Ghaderpoori, M. Metal-organic framework UiO-66 for adsorption of methylene blue dye from aqueous solutions. *Int. J. Environ. Sci. Technol.* **2017**, *14*, 1959–1968. <https://doi.org/10.1007/s13762-017-1289-z>.
83. He, Q.; Chen, Q.; Lü, M.; Liu, X. Adsorption Behavior of Rhodamine B on UiO-66. *Chin. J. Chem. Eng.* **2014**, *22*, 1285–1290. <https://doi.org/10.1016/j.cjche.2014.09.009>.
84. Molavi, H.; Hakimian, A.; Shojaei, A.; Raeiszadeh, M. Selective dye adsorption by highly water stable metal-organic framework: Long term stability analysis in aqueous media. *Appl. Surf. Sci.* **2018**, *445*, 424–436. <https://doi.org/10.1016/j.apsusc.2018.03.189>.
85. Yang, Q.; Wang, Y.; Wang, J.; Liu, F.; Hu, N.; Pei, H.; Yang, W.; Li, Z.; Suo, Y.; Wang, J. High effective adsorption/removal of illegal food dyes from contaminated aqueous solution by Zr-MOFs (UiO-67). *Food Chem.* **2018**, *254*, 241–248. <https://doi.org/10.1016/j.foodchem.2018.02.011>.
86. Li, H.; Cao, X.; Zhang, C.; Yu, Q.; Zhao, Z.; Niu, X.; Sun, X.; Liu, Y.; Ma, L.; Li, Z. Enhanced adsorptive removal of anionic and cationic dyes from single or mixed dye solutions using MOF PCN-222. *RSC Adv.* **2017**, *7*, 16273–16281. <https://doi.org/10.1039/C7RA01647F>.
87. Feng, Y.; Li, Y.; Xu, M.; Liu, S.; Yao, J. Fast adsorption of methyl blue on zeolitic imidazolate framework-8 and its adsorption mechanism. *RSC Adv.* **2016**, *6*, 109608–109612. <https://doi.org/10.1039/C6RA23870J>.
88. Lin, K.-Y.A.; Chang, H.-A. Ultra-high adsorption capacity of zeolitic imidazole framework-67 (ZIF-67) for removal of malachite green from water. *Chemosphere* **2015**, *139*, 624–631. <https://doi.org/10.1016/j.chemosphere.2015.01.041>.
89. Lin, S.; Song, Z.; Che, G.; Ren, A.; Li, P.; Liu, C.; Zhang, J. Adsorption behavior of metal–organic frameworks for methylene blue from aqueous solution. *Microporous Mesoporous Mater.* **2014**, *193*, 27–34. <https://doi.org/10.1016/j.micromeso.2014.03.004>.
90. Haque, E.; Jun, J.W.; Jhung, S.H. Adsorptive removal of methyl orange and methylene blue from aqueous solution with a metal-organic framework material, iron terephthalate (MOF-235). *J. Hazard. Mater.* **2011**, *185*, 507–511. <https://doi.org/10.1016/j.jhazmat.2010.09.035>.
91. Lu, H.; Zhang, L.; Wang, B.; Long, Y.; Zhang, M.; Ma, J.; Khan, A.; Chowdhury, S.P.; Zhou, X.; Ni, Y. Cellulose-supported magnetic Fe₃O₄-MOF composites for enhanced dye removal application. *Cellulose* **2019**, *26*, 4909–4920. <https://doi.org/10.1007/s10570-019-02415-y>.
92. Ge, J.; Wu, Z.; Huang, X.; Ding, M. An Effective Microwave-Assisted Synthesis of MOF235 with Excellent Adsorption of Acid Chrome Blue K. *J. Nanomater.* **2019**, *2019*, 4035075. <https://doi.org/10.1155/2019/4035075>.
93. Hazrati, M.; Safari, M. Cadmium-based metal–organic framework for removal of dye from aqueous solution. *Environ. Prog. Sustain. Energy* **2020**, *39*, e13411. <https://doi.org/10.1002/ep.13411>.
94. Masoomi, M.Y.; Bagheri, M.; Morsali, A. Porosity and dye adsorption enhancement by ultrasonic synthesized Cd(II) based metal-organic framework. *Ultrason. Sonochem.* **2017**, *37*, 244–250. <https://doi.org/10.1016/j.ultsonch.2017.01.018>.
95. Liu, Y.; Liu, Y.; Qu, R.; Ji, C.; Sun, C. Comparison of adsorption properties for anionic dye by metal organic frameworks with different metal ions. *Colloids Surf. A Physicochem. Eng. Asp.* **2020**, *586*, 124259. <https://doi.org/10.1016/j.colsurfa.2019.124259>.
96. Jung, K.-W.; Choi, B.H.; Dao, C.M.; Lee, Y.J.; Choi, J.-W.; Ahn, K.-H.; Lee, S.-H. Aluminum carboxylate-based metal organic frameworks for effective adsorption of anionic azo dyes from aqueous media. *J. Ind. Eng. Chem.* **2018**, *59*, 149–159. <https://doi.org/10.1016/j.jiec.2017.10.019>.
97. Al Sharabati, M.; Sabouni, R. Selective removal of dual dyes from aqueous solutions using a metal organic framework (MIL-53(Al)). *Polyhedron* **2020**, *190*, 114762. <https://doi.org/10.1016/j.poly.2020.114762>.
98. Jia, Y.; Jin, Q.; Li, Y.; Sun, Y.; Huo, J.; Zhao, X. Investigation of the adsorption behaviour of different types of dyes on MIL-100(Fe) and their removal from natural water. *Anal. Methods* **2015**, *7*, 1463–1470.
99. Kónya, Z.; Vessélényi, I.; Kiss, J.; Farkas, A.; Oszkó, A.; Kiricsi, I. XPS study of multiwall carbon nanotube synthesis on Ni-, V-, and Ni, V-ZSM-5 catalysts. *Appl. Catal. A Gen.* **2004**, *260*, 55–61. <https://doi.org/10.1016/j.apcata.2003.10.042>.
100. Kukovec, Á.; Kordás, K.; Kiss, J.; Kónya, Z. Atomic scale characterization and surface chemistry of metal modified titanate nanotubes and nanowires. *Surf. Sci. Rep.* **2016**, *71*, 473–546. <https://doi.org/10.1016/j.surfrep.2016.06.001>.
101. Jajko, G.; Kozyra, P.; Gutiérrez-Sevillano, J.J.; Makowski, W.; Calero, S. Carbon dioxide capture enhanced by pre-adsorption of water and methanol in UiO-66. *Chem. Eur. J.* **2021**, *27*, 14653–14659. <https://doi.org/10.1002/chem.202102181>.
102. Vahabi, A.H.; Norouzi, F.; Sheibani, E.; Rahimi-Nasrabadi, M. Functionalized Zr-UiO-67 metal-organic frameworks: Structural landscape and application. *Coord. Chem. Rev.* **2021**, *445*, 214050. <https://doi.org/10.1016/j.ccr.2021.214050>.

103. Ye, X.; Liu, D. Metal–Organic Framework UiO-68 and Its Derivatives with Sufficiently Good Properties and Performance Show Promising Prospects in Potential Industrial Applications. *Cryst. Growth Des.* **2021**, *21*, 4780–4804. <https://doi.org/10.1021/acs.cgd.1c00460>.
104. Zhao, X.; Zhao, H.; Dai, W.; Wei, Y.; Wang, Y.; Zhang, Y.; Zhi, L.; Huang, H.; Gao, Z. A metal-organic framework with large 1-D channels and rich OH sites for high-efficiency chloramphenicol removal from water. *J. Colloid Interface Sci.* **2018**, *526*, 28–34. <https://doi.org/10.1016/j.jcis.2018.04.095>.
105. Zhang, M.; Chen, Y.P.; Bosch, M.; Gentle, T., 3rd; Wang, K.; Feng, D.; Wang, Z.U.; Zhou, H.C. Symmetry-guided synthesis of highly porous metal-organic frameworks with fluorite topology. *Angew. Chem.* **2014**, *53*, 815–818. <https://doi.org/10.1002/anie.201307340>.
106. Lin, S.; Zhao, Y.; Yun, Y.-S. Highly Effective Removal of Nonsteroidal Anti-inflammatory Pharmaceuticals from Water by Zr(IV)-Based Metal–Organic Framework: Adsorption Performance and Mechanisms. *ACS Appl. Mater. Interfaces* **2018**, *10*, 28076–28085. <https://doi.org/10.1021/acsami.8b08596>.
107. Furukawa, H.; Gándara, F.; Zhang, Y.B.; Jiang, J.; Queen, W.L.; Hudson, M.R.; Yaghi, O.M. Water adsorption in porous metal-organic frameworks and related materials. *J. Am. Chem. Soc.* **2014**, *136*, 4369–4381. <https://doi.org/10.1021/ja500330a>.
108. Akpınar, I.; Drout, R.J.; Islamoglu, T.; Kato, S.; Lyu, J.; Farha, O.K. Exploiting π – π Interactions to Design an Efficient Sorbent for Atrazine Removal from Water. *ACS Appl. Mater. Interfaces* **2019**, *11*, 6097–6103. <https://doi.org/10.1021/acsami.8b20355>.
109. Gutov, O.V.; Bury, W.; Gomez-Gualdrón, D.A.; Krungleviciute, V.; Fairen-Jimenez, D.; Mondloch, J.E.; Sarjeant, A.A.; Al-Juaid, S.S.; Snurr, R.Q.; Hupp, J.T.; et al. Water-Stable Zirconium-Based Metal–Organic Framework Material with High-Surface Area and Gas-Storage Capacities. *Chem. Eur. J.* **2014**, *20*, 12389–12393. <https://doi.org/10.1002/chem.201402895>.
110. Bai, Y.; Dou, Y.; Xie, L.-H.; Rutledge, W.; Li, J.-R.; Zhou, H.-C. Zr-based metal–organic frameworks: Design, synthesis, structure, and applications. *Chem. Soc. Rev.* **2016**, *45*, 2327–2367. <https://doi.org/10.1039/C5CS00837A>.
111. Chen, B.; Yang, Z.; Zhu, Y.; Xia, Y. Zeolitic imidazolate framework materials: Recent progress in synthesis and applications. *J. Mater. Chem. A* **2014**, *2*, 16811–16831. <https://doi.org/10.1039/C4TA02984D>.
112. Fairen-Jimenez, D.; Moggach, S.A.; Wharmby, M.T.; Wright, P.A.; Parsons, S.; Düren, T. Opening the gate: Framework flexibility in ZIF-8 explored by experiments and simulations. *J. Am. Chem. Soc.* **2011**, *133*, 8900–8902. <https://doi.org/10.1021/ja202154j>.
113. Wang, F.; Tan, Y.-X.; Yang, H.; Zhang, H.-X.; Kang, Y.; Zhang, J. A new approach towards tetrahedral imidazolate frameworks for high and selective CO₂ uptake. *Chem. Commun.* **2011**, *47*, 5828–5830. <https://doi.org/10.1039/C1CC10829H>.
114. Santoso, E.; Ediati, R.; Istiqomah, Z.; Sulistiono, D.O.; Nugraha, R.E.; Kusumawati, Y.; Bahruji, H.; Prasetyoko, D. Facile synthesis of ZIF-8 nanoparticles using polar acetic acid solvent for enhanced adsorption of methylene blue. *Microporous Mesoporous Mater.* **2021**, *310*, 110620. <https://doi.org/10.1016/j.micromeso.2020.110620>.
115. Oveisi, M.; Asli, M.A.; Mahmoodi, N.M. MIL-Ti metal-organic frameworks (MOFs) nanomaterials as superior adsorbents: Synthesis and ultrasound-aided dye adsorption from multicomponent wastewater systems. *J. Hazard. Mater.* **2018**, *347*, 123–140. <https://doi.org/10.1016/j.jhazmat.2017.12.057>.
116. Dias, E.M.; Petit, C. Towards the use of metal–organic frameworks for water reuse: A review of the recent advances in the field of organic pollutants removal and degradation and the next steps in the field. *J. Mater. Chem. A* **2015**, *3*, 22484–22506. <https://doi.org/10.1039/C5TA05440K>.
117. Bosch, M.; Zhang, M.; Zhou, H.-C. Increasing the Stability of Metal-Organic Frameworks. *Adv. Chem.* **2014**, *2014*, 182327. <https://doi.org/10.1155/2014/182327>.
118. Zhu, A.; Xuan, T.; Zhai, Y.; Wu, Y.; Guo, X.; Ying, Y.; Wen, Y.; Yang, H. Preparation of magnetic metal organic framework: A magnetically induced improvement effect for detection of parathion-methyl. *Sens. Actuators B Chem.* **2021**, *339*, 129909. <https://doi.org/10.1016/j.snb.2021.129909>.
119. Hong, Y.-s.; Sun, S.-l.; Sun, Q.; Gao, E.-Q.; Ye, M. Tuning adsorption capacity through ligand pre-modification in functionalized Zn-MOF analogues. *Mater. Chem. Phys.* **2020**, *243*, 122601. <https://doi.org/10.1016/j.matchemphys.2019.122601>.
120. Haque, E.; Lo, V.; Minett, A.I.; Harris, A.T.; Church, T.L. Dichotomous adsorption behaviour of dyes on an amino-functionalised metal–organic framework, amino-MIL-101(Al). *J. Mater. Chem. A* **2014**, *2*, 193–203. <https://doi.org/10.1039/C3TA13589F>.
121. Haque, E.; Lee, J.E.; Jang, I.T.; Hwang, Y.K.; Chang, J.-S.; Jegal, J.; Jhung, S.H. Adsorptive removal of methyl orange from aqueous solution with metal-organic frameworks, porous chromium-benzenedicarboxylates. *J. Hazard. Mater.* **2010**, *181*, 535–542. <https://doi.org/10.1016/j.jhazmat.2010.05.047>.
122. Xing, M.; Wang, J. Nanoscaled zero valent iron/graphene composite as an efficient adsorbent for Co(II) removal from aqueous solution. *J. Colloid Interface Sci.* **2016**, *474*, 119–128. <https://doi.org/10.1016/j.jcis.2016.04.031>.
123. Ye, Z.; Padilla, J.A.; Xuriguera, E.; Brillas, E.; Sirés, I. Magnetic MIL(Fe)-type MOF-derived N-doped nano-ZVI@C rods as heterogeneous catalyst for the electro-Fenton degradation of gemfibrozil in a complex aqueous matrix. *Appl. Catal. B Environ.* **2020**, *266*, 118604. <https://doi.org/10.1016/j.apcatb.2020.118604>.
124. Mattingly, S.J.; O’Toole, M.G.; James, K.T.; Clark, G.J.; Nantz, M.H. Magnetic Nanoparticle-Supported Lipid Bilayers for Drug Delivery. *Langmuir* **2015**, *31*, 3326–3332. <https://doi.org/10.1021/la504830z>.
125. Hamedi, A.; Zarandi, M.B.; Nateghi, M.R. Highly efficient removal of dye pollutants by MIL-101(Fe) metal-organic framework loaded magnetic particles mediated by Poly L-Dopa. *J. Environ. Chem. Eng.* **2019**, *7*, 102882. <https://doi.org/10.1016/j.jece.2019.102882>.
126. Jiao, C.; Wang, Y.; Li, M.; Wu, Q.; Wang, C.; Wang, Z. Synthesis of magnetic nanoporous carbon from metal-organic framework for the fast removal of organic dye from aqueous solution. *J. Magn. Magn. Mater.* **2016**, *407*, 24–30. <https://doi.org/10.1016/j.jmmm.2016.01.031>.

127. Ke, F.; Yuan, Y.-P.; Qiu, L.-G.; Shen, Y.-H.; Xie, A.-J.; Zhu, J.-F.; Tian, X.-Y.; Zhang, L.-D. Facile fabrication of magnetic metal–organic framework nanocomposites for potential targeted drug delivery. *J. Mater. Chem.* **2011**, *21*, 3843–3848. <https://doi.org/10.1039/C0JM01770A>.
128. Silvestre, M.E.; Franzreb, M.; Weidler, P.G.; Shekhah, O.; Wöll, C. Magnetic Cores with Porous Coatings: Growth of Metal–Organic Frameworks on Particles Using Liquid Phase Epitaxy. *Adv. Funct. Mater.* **2013**, *23*, 1210–1213. <https://doi.org/10.1002/adfm.201202078>.
129. Zhang, C.-F.; Qiu, L.-G.; Ke, F.; Zhu, Y.-J.; Yuan, Y.-P.; Xu, G.-S.; Jiang, X. A novel magnetic recyclable photocatalyst based on a core–shell metal–organic framework Fe₃O₄@MIL-100(Fe) for the decolorization of methylene blue dye. *J. Mater. Chem. A* **2013**, *1*, 14329–14334. <https://doi.org/10.1039/C3TA13030D>.
130. Huang, Y.-F.; Wang, Y.-Q.; Zhao, Q.-S.; Li, Y.; Zhang, J.-M. Facile in situ hydrothermal synthesis of Fe₃O₄@MIL-101 composites for removing textile dyes. *RSC Adv.* **2014**, *4*, 47921–47924. <https://doi.org/10.1039/C4RA05515B>.
131. Lu, G.; Li, S.; Guo, Z.; Farha, O.K.; Hauser, B.G.; Qi, X.; Wang, Y.; Wang, X.; Han, S.; Liu, X.; et al. Imparting functionality to a metal–organic framework material by controlled nanoparticle encapsulation. *Nat. Chem.* **2012**, *4*, 310–316. <https://doi.org/10.1038/nchem.1272>.
132. Lohe, M.R.; Gedrich, K.; Freudenberg, T.; Kockrick, E.; Dellmann, T.; Kaskel, S. Heating and separation using nanomagnet-functionalized metal–organic frameworks. *Chem. Commun.* **2011**, *47*, 3075–3077. <https://doi.org/10.1039/C0CC05278G>.
133. Doherty, C.M.; Knystautas, E.; Buso, D.; Villanova, L.; Konstas, K.; Hill, A.J.; Takahashi, M.; Falcaro, P. Magnetic framework composites for polycyclic aromatic hydrocarbon sequestration. *J. Mater. Chem.* **2012**, *22*, 11470–11474. <https://doi.org/10.1039/C2JM31798B>.
134. Bradshaw, D.; Garai, A.; Huo, J. Metal–organic framework growth at functional interfaces: Thin films and composites for diverse applications. *Chem. Soc. Rev.* **2012**, *41*, 2344–2381. <https://doi.org/10.1039/C1CS15276A>.
135. Senosy, I.A.; Zhang, X.-Z.; Lu, Z.-H.; Guan, X.-Y.; Yang, Z.-H.; Li, J.-H.; Guo, H.-M.; Abdelrahman, T.M.; Mmby, M.; Gbilyi, A. Magnetic metal-organic framework MIL-100 (Fe)/polyethyleneimine composite as an adsorbent for the magnetic solid-phase extraction of fungicides and their determination using HPLC-UV. *Microchim. Acta* **2021**, *188*, 33. <https://doi.org/10.1007/s00604-020-04648-2>.
136. Min, X.; Yang, W.; Hui, Y.-F.; Gao, C.-Y.; Dang, S.; Sun, Z.-M. Fe₃O₄@ZIF-8: A magnetic nanocomposite for highly efficient UO₂²⁺ adsorption and selective UO₂²⁺/Ln³⁺ separation. *Chem. Commun.* **2017**, *53*, 4199–4202. <https://doi.org/10.1039/C6CC10274C>.
137. Vo, T.K.; Kim, J. Facile synthesis of magnetic framework composite MgFe₂O₄@UiO-66(Zr) and its applications in the adsorption–photocatalytic degradation of tetracycline. *Environ. Sci. Pollut. Res.* **2021**, *28*, 68261–68275. <https://doi.org/10.1007/s11356-021-15423-y>.
138. Cai, Y.; Feng, J.; Tan, X.; Wang, X.; Lv, Z.; Chen, W.; Fang, M.; Liu, H.; Wang, X. Efficient capture of ReO₄[−] on magnetic amine-functionalized MIL-101(Cr): Revealing from selectivity to mechanism. *Sci. Total Environ.* **2021**, *771*, 144840. <https://doi.org/10.1016/j.scitotenv.2020.144840>.
139. Liu, H.; Ren, X.; Chen, L. Synthesis and characterization of magnetic metal–organic framework for the adsorptive removal of Rhodamine B from aqueous solution. *J. Ind. Eng. Chem.* **2016**, *34*, 278–285. <https://doi.org/10.1016/j.jiec.2015.11.020>.
140. Abdi, J.; Mahmoodi, N.M.; Vossoughi, M.; Alemzadeh, I. Synthesis of magnetic metal-organic framework nanocomposite (ZIF-8@SiO₂@MnFe₂O₄) as a novel adsorbent for selective dye removal from multicomponent systems. *Microporous Mesoporous Mater.* **2019**, *273*, 177–188. <https://doi.org/10.1016/j.micromeso.2018.06.040>.
141. Wang, T.; Zhao, P.; Lu, N.; Chen, H.; Zhang, C.; Hou, X. Facile fabrication of Fe₃O₄/MIL-101(Cr) for effective removal of acid red 1 and orange G from aqueous solution. *Chem. Eng. J.* **2016**, *295*, 403–413. <https://doi.org/10.1016/j.cej.2016.03.016>.
142. Shi, Z.; Xu, C.; Guan, H.; Li, L.; Fan, L.; Wang, Y.; Liu, L.; Meng, Q.; Zhang, R. Magnetic metal organic frameworks (MOFs) composite for removal of lead and malachite green in wastewater. *Colloids Surf. A Physicochem. Eng. Asp.* **2018**, *539*, 382–390. <https://doi.org/10.1016/j.colsurfa.2017.12.043>.
143. Xu, Y.; Jin, J.; Li, X.; Song, C.; Meng, H.; Zhang, X. Adsorption behavior of methylene blue on Fe₃O₄-embedded hybrid magnetic metal–organic framework. *Desalin. Water Treat.* **2016**, *57*, 25216–25225. <https://doi.org/10.1080/19443994.2016.1148639>.
144. Jiang, Z.; Li, Y. Facile synthesis of magnetic hybrid Fe₃O₄/MIL-101 via heterogeneous coprecipitation assembly for efficient adsorption of anionic dyes. *J. Taiwan Inst. Chem. Eng.* **2016**, *59*, 373–379. <https://doi.org/10.1016/j.jtice.2015.09.002>.
145. Zhao, X.; Liu, S.; Tang, Z.; Niu, H.; Cai, Y.; Meng, W.; Wu, F.; Giesy, J.P. Synthesis of magnetic metal-organic framework (MOF) for efficient removal of organic dyes from water. *Sci. Rep.* **2015**, *5*, 11849. <https://doi.org/10.1038/srep11849>.
146. Han, L.-J.; Ge, F.-Y.; Sun, G.-H.; Gao, X.-J.; Zheng, H.-G. Effective adsorption of Congo red by a MOF-based magnetic material. *Dalton Trans.* **2019**, *48*, 4650–4656. <https://doi.org/10.1039/C9DT00813F>.
147. Lin, Y.; Yan, Q.; Kong, C.; Chen, L. Polyethyleneimine incorporated metal-organic frameworks adsorbent for highly selective CO₂ capture. *Sci. Rep.* **2013**, *3*, 1859. <https://doi.org/10.1038/srep01859>.
148. Eddaoudi, M.; Kim, J.; Rosi, N.; Vodak, D.; Wachter, J.; O’Keeffe, M.; Yaghi, O.M. Systematic design of pore size and functionality in isoreticular MOFs and their application in methane storage. *Science* **2002**, *295*, 469–472. <https://doi.org/10.1126/science.1067208>.
149. Gadzikwa, T.; Lu, G.; Stern, C.L.; Wilson, S.R.; Hupp, J.T.; Nguyen, S.T. Covalent surface modification of a metal–organic framework: Selective surface engineering via CuI-catalyzed Huisgen cycloaddition. *Chem. Commun.* **2008**, *44*, 5493–5495. <https://doi.org/10.1039/B805101A>.

150. Braun, M.E.; Steffek, C.D.; Kim, J.; Rasmussen, P.G.; Yaghi, O.M. 1,4-Benzenedicarboxylate derivatives as links in the design of paddle-wheel units and metal–organic frameworks. *Chem. Commun.* **2001**, *37*, 2532–2533. <https://doi.org/10.1039/B108031H>.
151. Serra-Crespo, P.; Ramos-Fernandez, E.V.; Gascon, J.; Kapteijn, F. Synthesis and Characterization of an Amino Functionalized MIL-101(Al): Separation and Catalytic Properties. *Chem. Mater.* **2011**, *23*, 2565–2572. <https://doi.org/10.1021/cm103644b>.
152. Vaidhyanathan, R.; Iremonger, S.S.; Dawson, K.W.; Shimizu, G.K.H. An amine-functionalized metal organic framework for preferential CO₂ adsorption at low pressures. *Chem. Commun.* **2009**, *45*, 5230–5232. <https://doi.org/10.1039/B911481E>.
153. Yan, Q.; Lin, Y.; Wu, P.; Zhao, L.; Cao, L.; Peng, L.; Kong, C.; Chen, L. Designed Synthesis of Functionalized Two-Dimensional Metal–Organic Frameworks with Preferential CO₂ Capture. *ChemPlusChem* **2013**, *78*, 86–91. <https://doi.org/10.1002/cplu.201200270>.
154. Lin, R.-B.; Chen, D.; Lin, Y.-Y.; Zhang, J.-P.; Chen, X.-M. A Zeolite-Like Zinc Triazolate Framework with High Gas Adsorption and Separation Performance. *Inorg. Chem.* **2012**, *51*, 9950–9955. <https://doi.org/10.1021/ic301463z>.
155. Liu, H.; Chen, L.; Ding, J. Adsorption behavior of magnetic amino-functionalized metal–organic framework for cationic and anionic dyes from aqueous solution. *RSC Adv.* **2016**, *6*, 48884–48895. <https://doi.org/10.1039/C6RA07567C>.
156. Zhang, W.; Zhang, R.-Z.; Yin, Y.; Yang, J.-M. Superior selective adsorption of anionic organic dyes by MIL-101 analogs: Regulation of adsorption driving forces by free amino groups in pore channels. *J. Mol. Liq.* **2020**, *302*, 112616. <https://doi.org/10.1016/j.molliq.2020.112616>.
157. Bibi, R.; Wei, L.; Shen, Q.; Tian, W.; Oderinde, O.; Li, N.; Zhou, J. Effect of Amino Functionality on the Uptake of Cationic Dye by Titanium-Based Metal Organic Frameworks. *J. Chem. Eng. Data* **2017**, *62*, 1615–1622. <https://doi.org/10.1021/acs.jced.6b01012>.
158. Bao, S.; Li, K.; Ning, P.; Peng, J.; Jin, X.; Tang, L. Synthesis of amino-functionalization magnetic multi-metal organic framework (Fe₃O₄/MIL-101(Al_{0.9}Fe_{0.1})/NH₂) for efficient removal of methyl orange from aqueous solution. *J. Taiwan Inst. Chem. Eng.* **2018**, *87*, 64–72. <https://doi.org/10.1016/j.jtice.2018.03.009>.
159. Karimi, M.A.; Masroui, H.; Mirbagheri, M.A.; Andishgar, S.; Pourshamsi, T. Synthesis of a new magnetic metal–organic framework nanocomposite and its application in methylene blue removal from aqueous solution. *JCCS J. Chin. Chem. Soc.* **2018**, *65*, 1229–1238. <https://doi.org/10.1002/jccs.201800061>.
160. Tambat, S.N.; Sane, P.K.; Suresh, S.; Varadan, O.N.; Pandit, A.B.; Sontakke, S.M. Hydrothermal synthesis of NH₂-UiO-66 and its application for adsorptive removal of dye. *Adv. Powder Technol.* **2018**, *29*, 2626–2632. <https://doi.org/10.1016/j.apt.2018.07.010>.
161. Li, L.; Liu, X.L.; Geng, H.Y.; Hu, B.; Song, G.W.; Xu, Z.S. A MOF/graphite oxide hybrid (MOF: HKUST-1) material for the adsorption of methylene blue from aqueous solution. *J. Mater. Chem. A* **2013**, *1*, 10292–10299. <https://doi.org/10.1039/C3TA11478C>.
162. Huang, X.; Tan, C.; Yin, Z.; Zhang, H. 25th Anniversary Article: Hybrid Nanostructures Based on Two-Dimensional Nanomaterials. *Adv. Mater.* **2014**, *26*, 2185–2204. <https://doi.org/10.1002/adma.201304964>.
163. Kumar, R.; Jayaramulu, K.; Maji, T.K.; Rao, C.N.R. Hybrid nanocomposites of ZIF-8 with graphene oxide exhibiting tunable morphology, significant CO₂ uptake and other novel properties. *Chem. Commun.* **2013**, *49*, 4947–4949. <https://doi.org/10.1039/C3CC00136A>.
164. Petit, C.; Bandoz, T.J. MOF–graphite oxide nanocomposites: Surface characterization and evaluation as adsorbents of ammonia. *J. Mater. Chem.* **2009**, *19*, 6521–6528. <https://doi.org/10.1039/B908862H>.
165. Huang, H.; Zhang, J.; Jiang, L.; Zang, Z. Preparation of cubic Cu₂O nanoparticles wrapped by reduced graphene oxide for the efficient removal of rhodamine B. *J. Alloys Compd.* **2017**, *718*, 112–115. <https://doi.org/10.1016/j.jallcom.2017.05.132>.
166. Tanhaei, M.; Mahjoub, A.R.; Safarifard, V. Sonochemical synthesis of amide-functionalized metal-organic framework/graphene oxide nanocomposite for the adsorption of methylene blue from aqueous solution. *Ultrason. Sonochem.* **2018**, *41*, 189–195. <https://doi.org/10.1016/j.ultsonch.2017.09.030>.
167. Anzar, N.; Hasan, R.; Tyagi, M.; Yadav, N.; Narang, J. Carbon nanotube—A review on Synthesis, Properties and plethora of applications in the field of biomedical science. *Sens. Int.* **2020**, *1*, 100003. <https://doi.org/10.1016/j.sintl.2020.100003>.
168. Soni, S.K.; Thomas, B.; Kar, V.R. A Comprehensive Review on CNTs and CNT-Reinforced Composites: Syntheses, Characteristics and Applications. *Mater. Today Commun.* **2020**, *25*, 101546. <https://doi.org/10.1016/j.mtcomm.2020.101546>.
169. Rajabi, M.; Mahanpoor, K.; Moradi, O. Removal of dye molecules from aqueous solution by carbon nanotubes and carbon nanotube functional groups: Critical review. *RSC Adv.* **2017**, *7*, 47083–47090. <https://doi.org/10.1039/C7RA09377B>.
170. Liu, F.; Chung, S.; Oh, G.; Seo, T.S. Three-Dimensional Graphene Oxide Nanostructure for Fast and Efficient Water-Soluble Dye Removal. *ACS Appl. Mater. Interfaces* **2012**, *4*, 922–927. <https://doi.org/10.1021/am201590z>.
171. Dadashi Firouzjaei, M.; Akbari Afkhami, F.; Rabbani Esfahani, M.; Turner, C.H.; Nejati, S. Experimental and molecular dynamics study on dye removal from water by a graphene oxide-copper-metal organic framework nanocomposite. *J. Water Process Eng.* **2020**, *34*, 101180. <https://doi.org/10.1016/j.jwpe.2020.101180>.
172. Abdi, J.; Vossoughi, M.; Mahmoodi, N.M.; Alemzadeh, I. Synthesis of metal-organic framework hybrid nanocomposites based on GO and CNT with high adsorption capacity for dye removal. *Chem. Eng. J.* **2017**, *326*, 1145–1158. <https://doi.org/10.1016/j.cej.2017.06.054>.
173. Zhao, S.; Chen, D.; Wei, F.; Chen, N.; Liang, Z.; Luo, Y. Removal of Congo red dye from aqueous solution with nickel-based metalorganic framework/graphene oxide composites prepared by ultrasonic wave-assisted ball milling. *Ultrason. Sonochem.* **2017**, *39*, 845–852.
174. Kumar, G.; Masram, D.T. Sustainable Synthesis of MOF-5@GO Nanocomposites for Efficient Removal of Rhodamine B from Water. *ACS Omega* **2021**, *6*, 9587–9599. <https://doi.org/10.1021/acsomega.1c00143>.
175. Wu, S.-C.; Yu, L.-L.; Xiao, F.-F.; You, X.; Yang, C.; Cheng, J.-H. Synthesis of aluminum-based MOF/graphite oxide composite and enhanced removal of methyl orange. *J. Alloys Compd.* **2017**, *724*, 625–632. <https://doi.org/10.1016/j.jallcom.2017.07.095>.

176. Luo, S.; Wang, J. MOF/graphene oxide composite as an efficient adsorbent for the removal of organic dyes from aqueous solution. *Environ. Sci. Pollut. Res.* **2018**, *25*, 5521–5528. <https://doi.org/10.1007/s11356-017-0932-z>.
177. Lin, K.-Y.A.; Yang, H.; Hsu, F.-K. Zr-Metal Organic Framework and Derivatives for Adsorptive and Photocatalytic Removal of Acid Dyes. *Water Environ. Res.* **2018**, *90*, 144–154. <https://doi.org/10.2175/106143017X15054988926604>.
178. Huang, L.; He, M.; Chen, B.; Hu, B. Magnetic Zr-MOFs nanocomposites for rapid removal of heavy metal ions and dyes from water. *Chemosphere* **2018**, *199*, 435–444. <https://doi.org/10.1016/j.chemosphere.2018.02.019>.
179. Ayati, A.; Shahrak, M.N.; Tanhaei, B.; Sillanpää, M. Emerging adsorptive removal of azo dye by metal–organic frameworks. *Chemosphere* **2016**, *160*, 30–44. <https://doi.org/10.1016/j.chemosphere.2016.06.065>.
180. Shakoor, S.; Nasar, A. Removal of methylene blue dye from artificially contaminated water using citrus limetta peel waste as a very low cost adsorbent. *J. Taiwan Inst. Chem. Eng.* **2016**, *66*, 154–163. <https://doi.org/10.1016/j.jtice.2016.06.009>.
181. Porkodi, K.; Vasanth Kumar, K. Equilibrium, kinetics and mechanism modeling and simulation of basic and acid dyes sorption onto jute fiber carbon: Eosin yellow, malachite green and crystal violet single component systems. *J. Hazard. Mater.* **2007**, *143*, 311–327. <https://doi.org/10.1016/j.jhazmat.2006.09.029>.
182. Tian, H.; Peng, J.; Lv, T.; Sun, C.; He, H. Preparation and performance study of MgFe₂O₄/metal–organic framework composite for rapid removal of organic dyes from water. *J. Solid State Chem.* **2018**, *257*, 40–48. <https://doi.org/10.1016/j.jssc.2017.09.017>.
183. Abd El Salam, H.M.; Zaki, T. Removal of hazardous cationic organic dyes from water using nickel-based metal-organic frameworks. *Inorg. Chim. Acta* **2018**, *471*, 203–210. <https://doi.org/10.1016/j.ica.2017.10.040>.
184. Alqadami, A.A.; Naushad, M.; Alothman, Z.A.; Ahamad, T. Adsorptive performance of MOF nanocomposite for methylene blue and malachite green dyes: Kinetics, isotherm and mechanism. *J. Environ. Manag.* **2018**, *223*, 29–36. <https://doi.org/10.1016/j.jenvman.2018.05.090>.
185. Dadfarnia, S.; Haji Shabani, A.; Moradi, S.E.; Emami, S. Methyl red removal from water by iron based metal-organic frameworks loaded onto iron oxide nanoparticle adsorbent. *Appl. Surf. Sci.* **2015**, *330*, 85–93. <https://doi.org/10.1016/j.apsusc.2014.12.196>.
186. Shao, Y.; Zhou, L.; Bao, C.; Ma, J.; Liu, M.; Wang, F. Magnetic responsive metal–organic frameworks nanosphere with core–shell structure for highly efficient removal of methylene blue. *Chem. Eng. J.* **2016**, *283*, 1127–1136. <https://doi.org/10.1016/j.cej.2015.08.051>.
187. Leus, K.; Bogaerts, T.; De Decker, J.; Depauw, H.; Hendrickx, K.; Vrielinck, H.; Van Speybroeck, V.; Van Der Voort, P. Systematic study of the chemical and hydrothermal stability of selected “stable” Metal Organic Frameworks. *Microporous Mesoporous Mater.* **2016**, *226*, 110–116. <https://doi.org/10.1016/j.micromeso.2015.11.055>.
188. Jiang, H.-L.; Feng, D.; Wang, K.; Gu, Z.-Y.; Wei, Z.; Chen, Y.-P.; Zhou, H.-C. An Exceptionally Stable, Porphyrinic Zr Metal–Organic Framework Exhibiting pH-Dependent Fluorescence. *J. Am. Chem. Soc.* **2013**, *135*, 13934–13938. <https://doi.org/10.1021/ja406844r>.
189. Liu, T.-F.; Feng, D.; Chen, Y.-P.; Zou, L.; Bosch, M.; Yuan, S.; Wei, Z.; Fordham, S.; Wang, K.; Zhou, H.-C. Topology-Guided Design and Syntheses of Highly Stable Mesoporous Porphyrinic Zirconium Metal–Organic Frameworks with High Surface Area. *J. Am. Chem. Soc.* **2015**, *137*, 413–419. <https://doi.org/10.1021/ja5111317>.
190. Wang, K.; Feng, D.; Liu, T.F.; Su, J.; Yuan, S.; Chen, Y.P.; Bosch, M.; Zou, X.; Zhou, H.C. A series of highly stable mesoporous metalloporphyrin Fe-MOFs. *J. Am. Chem. Soc.* **2014**, *136*, 13983–13986. <https://doi.org/10.1021/ja507269n>.
191. Naushad, M.; Abdullah Alothman, Z.; Rabiul Awual, M.; Alfadul, S.M.; Ahamad, T. Adsorption of rose Bengal dye from aqueous solution by amberlite Ira-938 resin: Kinetics, isotherms, and thermodynamic studies. *Desalin. Water Treat.* **2016**, *57*, 13527–13533. <https://doi.org/10.1080/19443994.2015.1060169>.
192. Hasan, Z.; Jeon, J.; Jhung, S.H. Adsorptive removal of naproxen and clofibric acid from water using metal-organic frameworks. *J. Hazard. Mater.* **2012**, *209–210*, 151–157. <https://doi.org/10.1016/j.jhazmat.2012.01.005>.
193. Al-Muhtaseb, A.a.H.; Ibrahim, K.A.; Albadarin, A.B.; Ali-khashman, O.; Walker, G.M.; Ahmad, M.N.M. Remediation of phenol-contaminated water by adsorption using poly(methyl methacrylate) (PMMA). *Chem. Eng. J.* **2011**, *168*, 691–699. <https://doi.org/10.1016/j.cej.2011.01.057>.
194. Mohammadi, N.; Khani, H.; Gupta, V.K.; Amereh, E.; Agarwal, S. Adsorption process of methyl orange dye onto mesoporous carbon material–kinetic and thermodynamic studies. *J. Colloid Interface Sci.* **2011**, *362*, 457–462. <https://doi.org/10.1016/j.jcis.2011.06.067>.
195. Doulati Ardejani, F.; Badii, K.; Limaee, N.Y.; Shafaei, S.Z.; Mirhabibi, A.R. Adsorption of Direct Red 80 dye from aqueous solution onto almond shells: Effect of pH, initial concentration and shell type. *J. Hazard. Mater.* **2008**, *151*, 730–737. <https://doi.org/10.1016/j.jhazmat.2007.06.048>.